Assessment of Trailing-Edge Surface-Normal Active Flow Control for Lift Enhancement on High-Lift Systems

Seyedeh Sheida Hosseini*, James R. L. Koch*, C. P. van Dam **, Shishir A. Pandya*, Jeffrey A. Housman*

***NASA Ames Research Center**

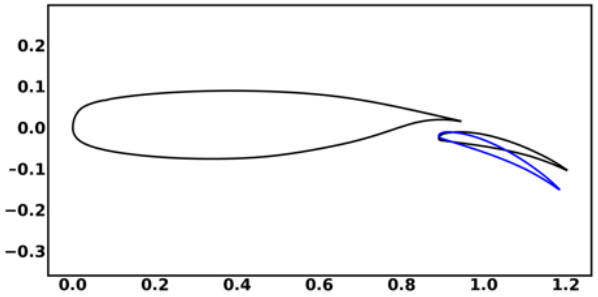
****University of California Davis**

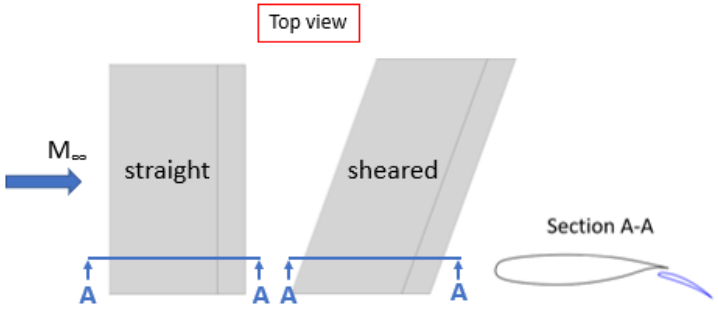
Advanced Modeling & Simulation (AMS) Seminar Series

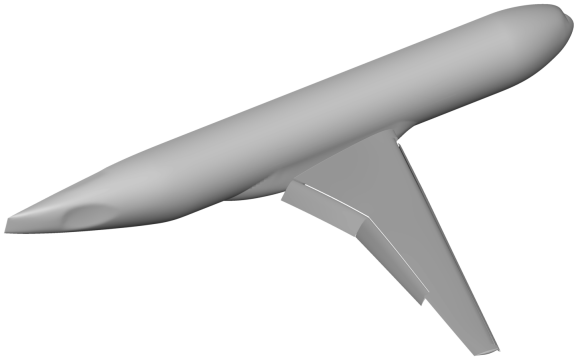
NASA Ames Research Center, March 16th, 2023

Outline

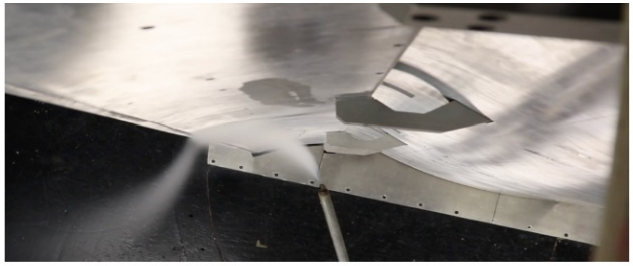
- Motivation
- Objectives and approach
- Summary of Results
  - Two dimensional studies
    - Computational
    - Wind tunnel
  - Three dimensional studies
    - Computational
  - Initial system feasibility analysis







Flap lower-side

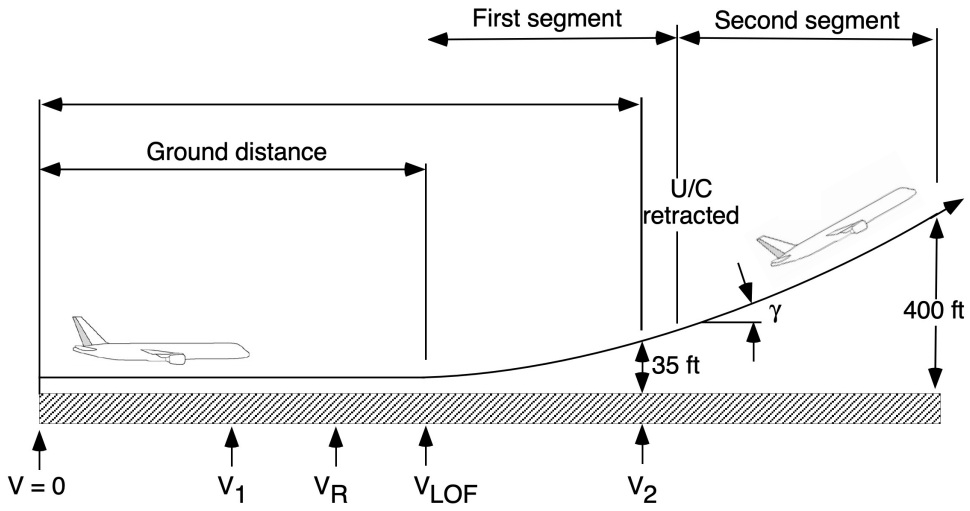


Source: Ed White et al., Texas A&M

Motivation

- Wing design for a wide range of airplane weights, fuselage lengths, airspeeds, and altitudes is challenging
- Airplanes are at high-lift conditions for relatively short periods, however high lift plays a critical role in aircraft safety, cost and economics
- High-lift systems generate higher lift coefficients to allow for reduced airspeed for shorter take-off and landing distances





AEO	=	All Engines Operating
OEI	=	One Engine Inoperative
V_{SR}	=	Reference stall speed (steady 1-g flight)
V_{LOF}	=	Lift-off speed
V_{MU}	=	Minimum unstick speed
V_{MC}	=	Minimum control speed
V_{MCG}	=	Minimum control speed on ground
V_R	=	Rotation speed
V_{SR}	=	Reference stall speed (steady 1-g flight)
V_1	=	Decision speed beyond which takeoff should no longer be aborted
V_2	=	Climb-out speed

Motivation

C_L at AOA in the linear regime

C_{Lmax}

$\frac{L}{D}$

V_1	≥	$1.20V_{MCG}$
V_R	≥	V_1
V_{LOF}	≥	$1.05^{a} V_{MC}$
	≥	$1.10 V_{MU}$ (AEO)
	≥	$1.05^{b} V_{MU}$ (OEI)
V_2	≥	$1.13 V_{SR}$
	≥	$1.10 V_{MC}$
$\tan\gamma$	≥	0.024 (twin, OEI)
	≥	0.027 (tri, OEI)
	≥	0.030 (quad, OEI)

AEO	=	All Engines Operating
OEI	=	One Engine Inoperative
V_{SR}	=	Reference stall speed (steady 1-g flight)
V_{LOF}	=	Lift-off speed
V_{MU}	=	Minimum unstick speed
V_{MC}	=	Minimum control speed
V_{MCG}	=	Minimum control speed on ground
V_R	=	Rotation speed
V_{SR}	=	Reference stall speed (steady 1-g flight)
V_1	=	Decision speed beyond which takeoff should no longer be aborted
V_2	=	Climb-out speed

[a])$1.08V_{MU}$ for geometrically limited airplane
[b])$1.04V_{MU}$ for geometrically limited airplane

Motivation

For a long range two-engine transport*,**:

- A 1.5% increase in $C_{L_{max}}$ ∝ 6,600 lb increase in payload (~ 33 passengers)
- A 1% increase in takeoff L/D ∝ 2,800 lb increase in payload (~14 passengers)
- A 0.1 increase in C_L at a constant angle of attack ∝ 1,400 lb reduction (~ 7 passengers) in airplane empty weight as a result of shortening the landing gear height by 14 in
  - At take-off C_L at a constant angle governs minimum unstick speed V_{MU}

C_L at AOA in the linear regime

C_{Lmax}

$\frac{L}{D}$

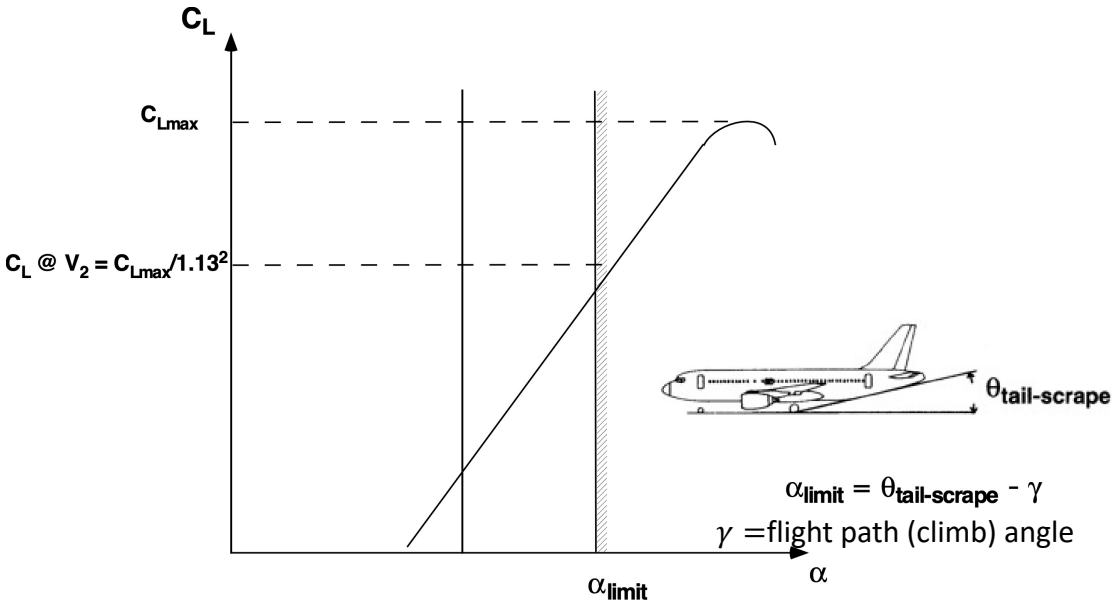
V_1	≥	$1.20V_{MCG}$
V_R	≥	V_1
	≥	$1.05_a V_{MC}$
V_{LOF}	≥	$1.10 V_{MU}$ (AEO)
	≥	$1.05^b V_{MU}$ (OEI)
$V_{2.}$	≥	$1.13 V_{SR}$
	≥	$1.10 V_{MC}$
$\tan\gamma$	≥	0.024 (twin, OEI)
	≥	0.027 (tri, OEI)
	≥	0.030 (quad, OEI)

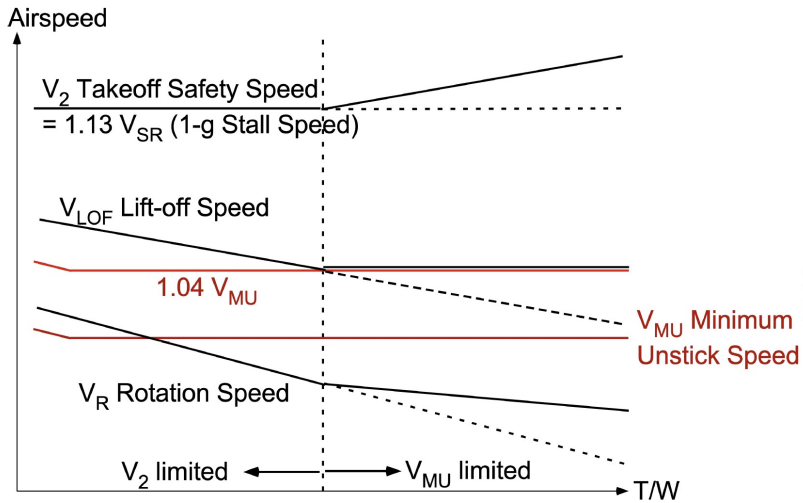
AEO	=	All Engines Operating
OEI	=	One Engine Inoperative
V_{SR}	=	Reference stall speed (steady 1-g flight)
V_{LOF}	=	Lift-off speed
V_{MU}	=	Minimum unstick speed
V_{MC}	=	Minimum control speed
V_{MCG}	=	Minimum control speed on ground
V_R	=	Rotation speed
V_{SR}	=	Reference stall speed (steady 1-g flight)
V_1	=	Decision speed beyond which takeoff should no longer be aborted
V_2	=	Climb-out speed

- *P. Meredith, "Viscous Phenomena Affecting High-Lift Systems and Suggestions for Future CFD Development. High-Lift System Aerodynamics," AGARD CP 515, pp. 19(1)–19(8), 1993.
- ** Shmilovich, Vijgen, Woszidlo, "Low-Speed Performance Enhancement using Localized AFC," NASA report. Apr 2022.

Motivation

- Example of limitations:
  - CL is limited by V2 requirements
  - AOA is limited by the tail scrape angle limiting CL
- If L = W can't be reached within the CL and AOA limit, Vmu increases which increases all major airspeeds, increasing the takeoff field length substantially
  - Due to negative impact on takeoff field length, high Vmu constraint may require redesign of flap system and/or landing gear.





* Adapted from: Slingerland, "Minimum Unstick Speed Calculation for High-Speed Jet Transport Aircraft," ICAS 2004

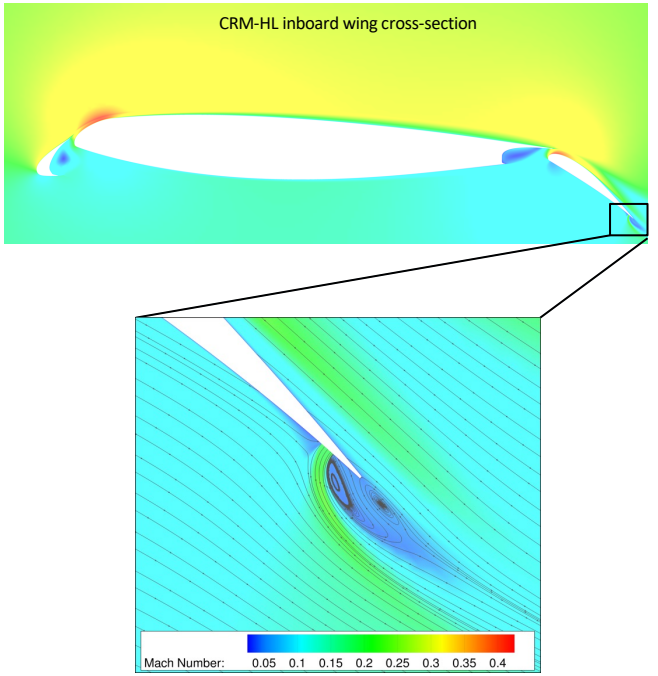
Surface-Normal Pneumatic AFC

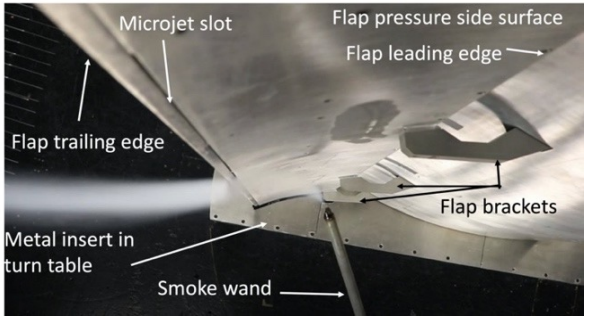
Objective

- Assess potential of surface-normal pneumatic AFC, microjets, for enhancing performance and control of lift of wing in high-lift configuration in the linear regime of the lift curve

Approach

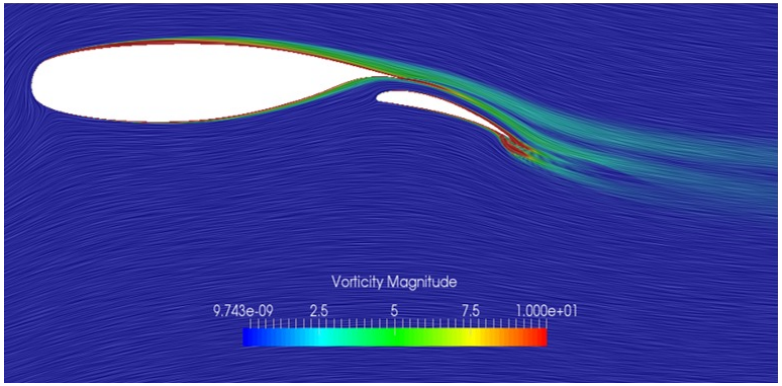
- Computational and experimental building-block approach to assess microjet enabled lift control at a range of flow conditions
  - Two-dimensional and infinite wing studies:
    - Microjet characteristics such as location, exit width, momentum coefficient, mass flow, continuous vs. pulsed blowing, solidity ratio and jet angle
    - Experiments in the Texas A&M Oran W. Nicks wind tunnel to validate the computational results and begin to assess system requirements
  - Three-dimensional studies on the high-lift Common Research Model (HL-CRM) to identify most promising microjet configurations
  - System analysis

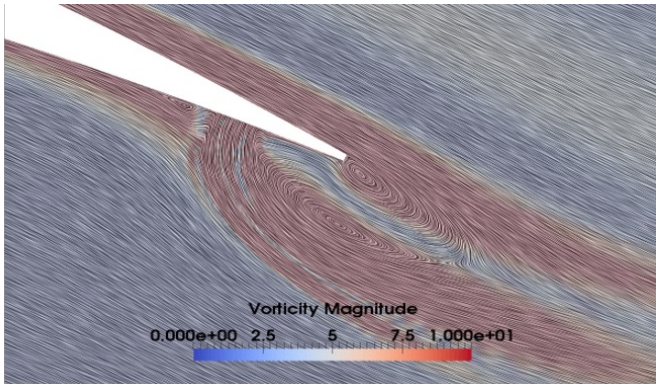




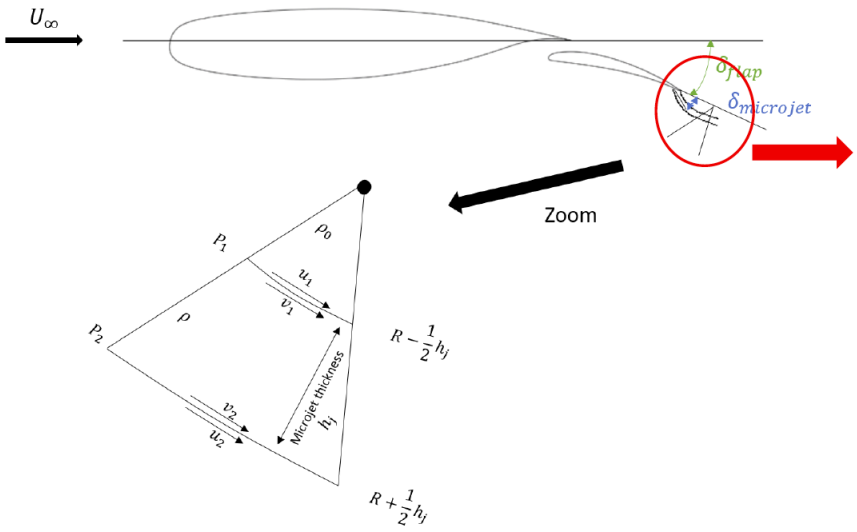
Source: Ed White et al., Texas A&M

Surface-Normal Pneumatic AFC, Theory



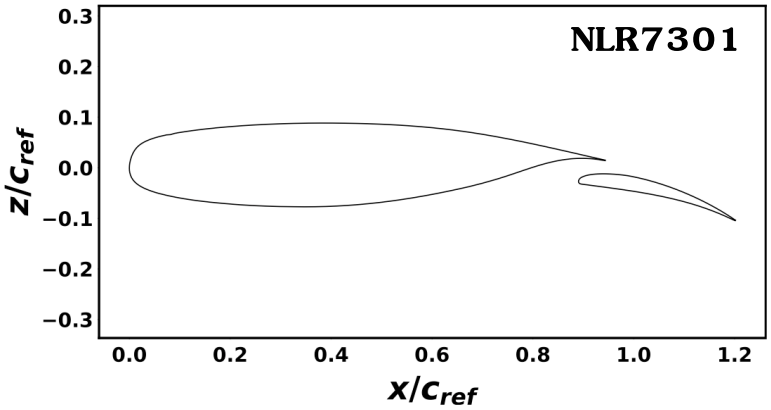


- Aerodynamic forces are modified:
  - i) Reaction due to the microjet momentum force
  - ii) Due to the modified pressure on the airfoil surface by the asymmetry the microjet creates in the flow-field
- Optimal location for circulation control effecting airfoil camber is at the wing trailing edge



Hosseini, Seyedeh Sheida, C. P. Van Dam, and Shishir A. Pandya. "Aerodynamic Load Control for Multi-Element Airfoils Using Surface-Normal Trailing-Edge Blowing." *Journal of Aircraft* 56.4 (2019): 1668-1676.

Summary of 2D computational studies



2D Computational Studies

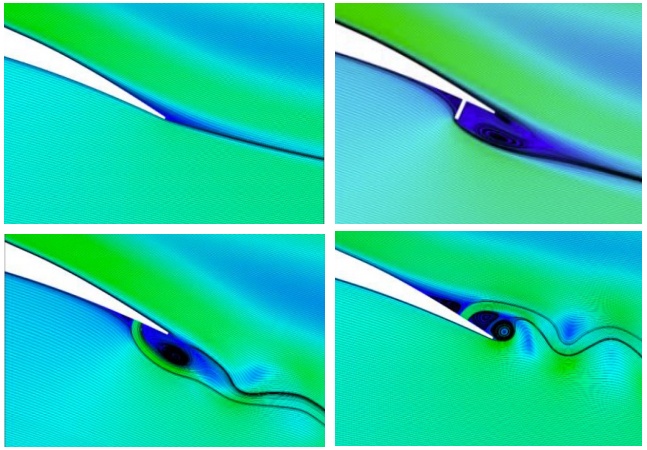
NLR 7301 two-element airfoil

- CFD validation / computational sensitivities using NASA's OVERFLOW and LAVA codes
  - Grid resolution, grid connectivity, N-S solver and turbulence model sensitivities
  - Far field grown 10,000c away from model
  - URANS with decreasing timestep restarts
  - OVERFLOW:
    - O-grid topology and DCF mesh connectivity
    - Third order central difference scheme, ARC3D diagonalized approx. factorization with matrix artificial dissipation
    - SST turbulence model (and SA-RC-QCR2000 for LAVA validation)
  - LAVA:
    - O-grid topology with trailing edge H-grids and LAVA connectivity
    - Second-order conservative finite-difference scheme, modified Roe scheme with third-order upwind-biased reconstruction and Koren limiter, BDF2 for physical time.
    - SA-RC-QCR2000 turbulence model

2D Computational Studies

Configuration and flow condition sensitivities studies

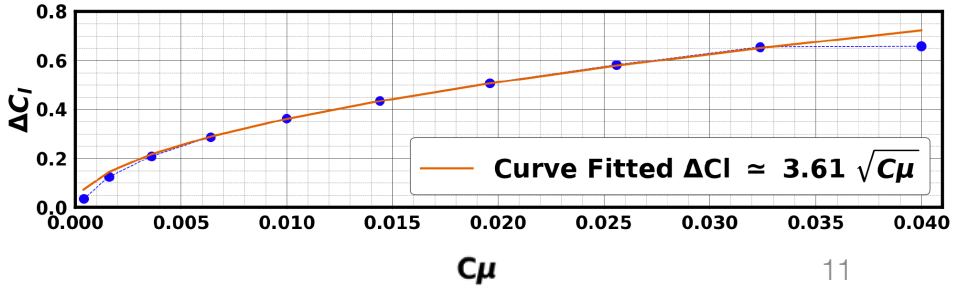
- Microjet and microtab comparison
- Microjets location (pressure-side vs. suction-side) effects over angle of attack range and drag decomposition analysis
- Control-volume based force analysis
- Microjet chordwise location and width
- Initial power requirement analysis
- Effects of modeling microjets with a boundary condition vs plenum on inlet velocity profile.
- Continuous vs. pulsed blowing effects
- Mach number and Reynolds number sensitivities
- Momentum coefficient sweeps ($\Delta C_l = K\sqrt{C_\mu}$ confirmed)
- Flap deflection angle, baseline 20 degrees and 30 degrees



'Normal Blowing' Assumed:

$$C\mu = \frac{\dot{m}_j U_j}{\frac{1}{2}\rho_\infty U_\infty^2 S_{ref}} \xrightarrow{\dot{m}_j = (\rho U A)_j} C\mu = \frac{\rho_j U_j^2 h_j b}{\frac{1}{2}\rho_\infty U_\infty^2 b\, c} \xrightarrow{Incompressible} C\mu = 2\frac{U_j^2}{U_\infty^2}\frac{h_j}{c}$$

- Microjet jet angle for 20 degree flap deflection



2D Computational Studies

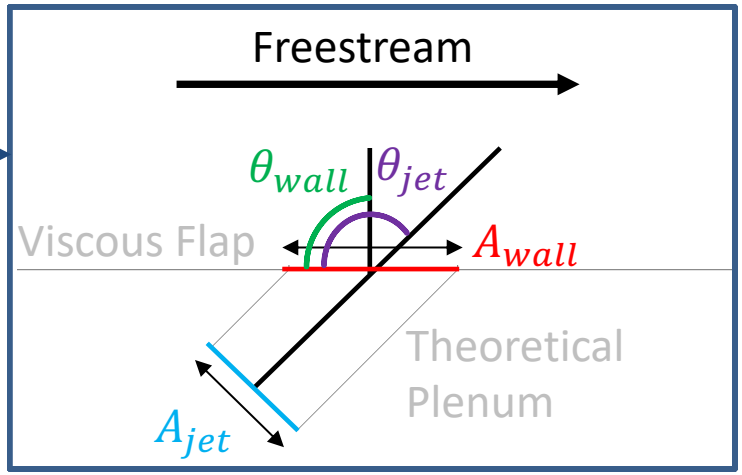
Angled Jet Methodology

- Jet incompressibility and normalcy to surface can no longer be assumed ($\rho_{jet} \neq \rho_{\infty}$ and $n_{jet} \neq n_{wall}$).

2D Computational Studies

Angled Jet Methodology

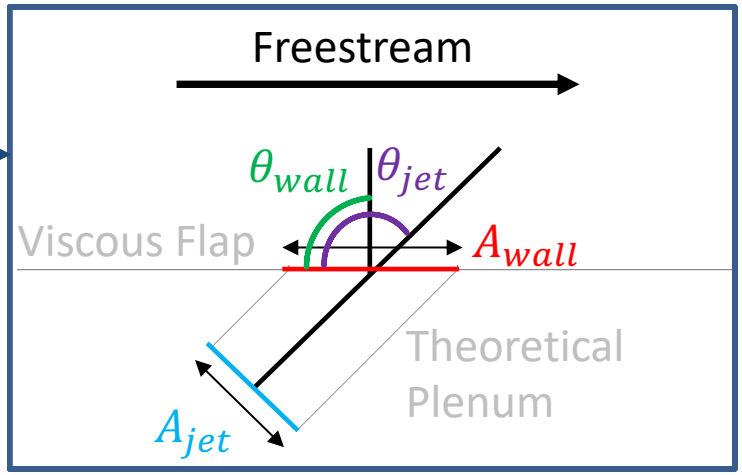
- Jet incompressibility and normalcy to surface can no longer be assumed ($\rho_{jet} \neq \rho_{\infty}$ and $n_{jet} \neq n_{wall}$).
- Angled jet requires exit area projection.



2D Computational Studies

Angled Jet Methodology

- Jet incompressibility and normalcy to surface can no longer be assumed ($\rho_{jet} \neq \rho_{\infty}$ and $n_{jet} \neq n_{wall}$).
- Angled jet requires exit area projection.
- Must define two of the following and solve for third:
  - C_{μ}
  - U
  - $mass\ parameter\ (\rho\ or\ \dot{m}\ -other\ can\ be\ calculated)$



Mass parameter of ρ:

$$C_{\mu,jet} = \frac{2\rho_{jet}A_{jet}U_{jet}^2(n_{wall} \cdot n_{jet})}{\rho_{\infty}A_{\infty}U_{\infty}^2}$$

Mass parameter of $\dot{m}$:

$$C_{\mu,jet} = \frac{2 * \dot{m}_{jet} * U_{jet}}{\dot{m}_{\infty} * U_{\infty}}$$

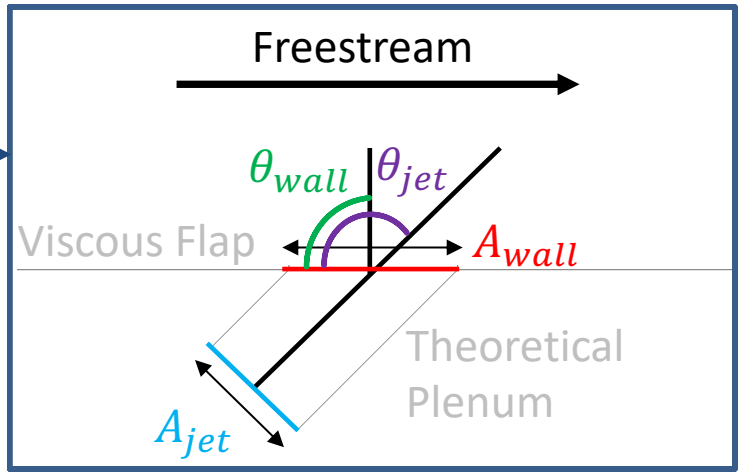
$$\dot{m}_{jet} = \rho_{jet} * A_{jet} * U_{jet} * (n_{wall} \cdot n_{jet})$$

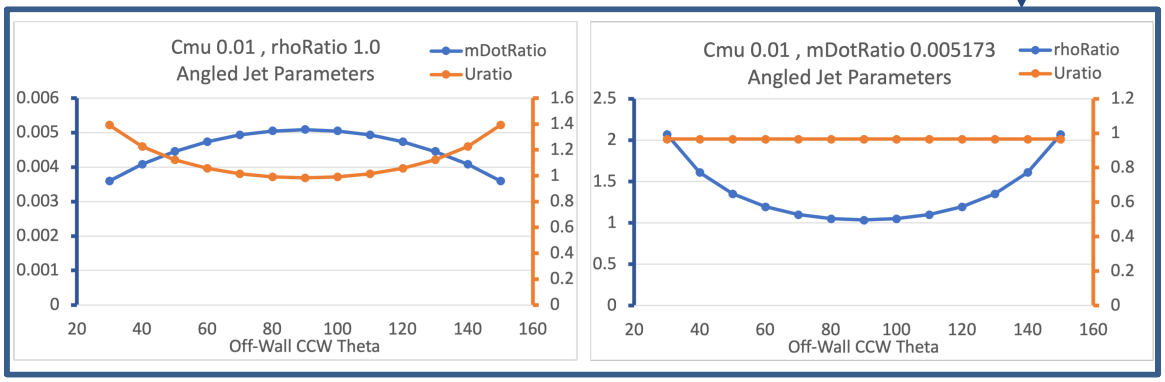
$$\dot{m}_{\infty} = \rho_{\infty} * A_{\infty} * U_{\infty}$$

2D Computational Studies

Angled Jet Methodology

- Jet incompressibility and normalcy to surface can no longer be assumed ($\rho_{jet} \neq \rho_{\infty}$ and $n_{jet} \neq n_{wall}$).
- Angled jet requires exit area projection.
- Must define two of the following and solve for third:
  - C_{μ}
  - U
  - $mass\ parameter\ (\rho\ or\ \dot{m}\ -other\ can\ be\ calculated)$
- Jet description differs based on mass parameter.





Mass parameter of ρ:

$$C_{\mu,jet} = \frac{2\rho_{jet}A_{jet}U_{jet}^2(n_{wall} \cdot n_{jet})}{\rho_{\infty}A_{\infty}U_{\infty}^2}$$

Mass parameter of $\dot{m}$:

$$C_{\mu,jet} = \frac{2 * \dot{m}_{jet} * U_{jet}}{\dot{m}_{\infty} * U_{\infty}}$$

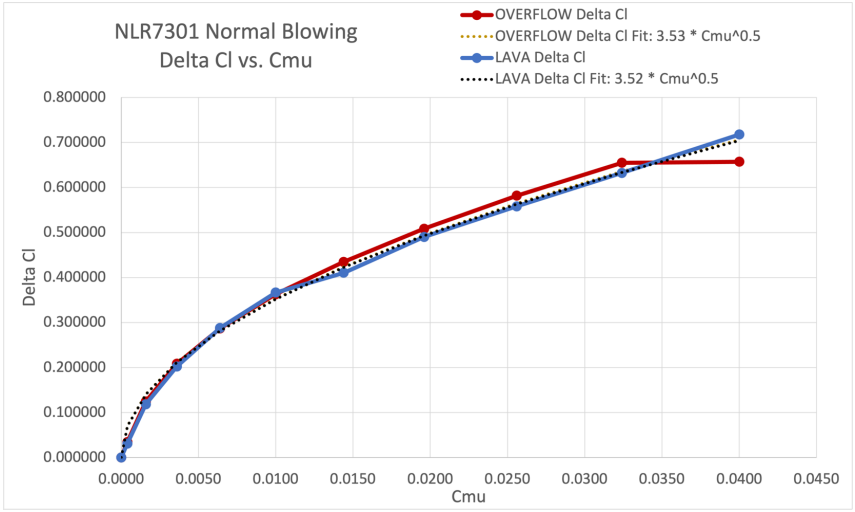
$$\dot{m}_{jet} = \rho_{jet} * A_{jet} * U_{jet} * (n_{wall} \cdot n_{jet})$$

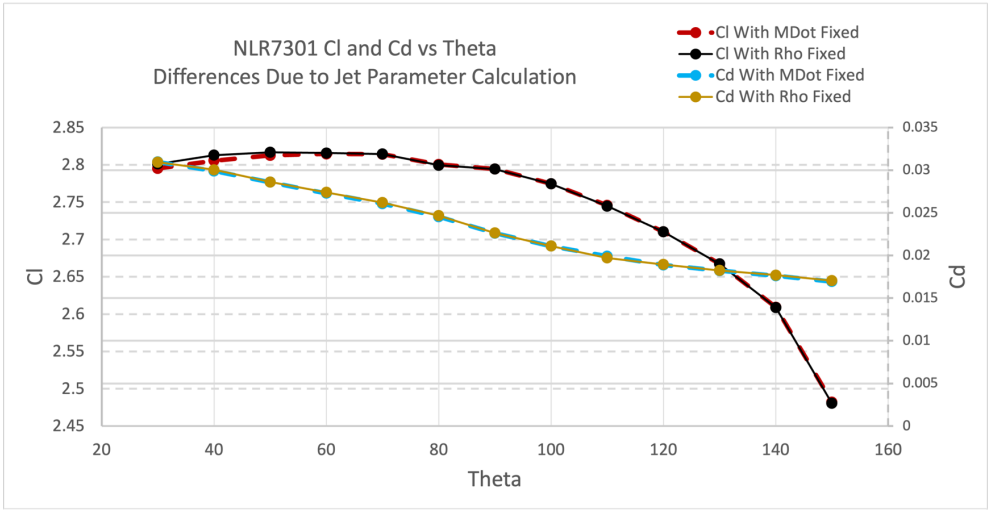
$$\dot{m}_{\infty} = \rho_{\infty} * A_{\infty} * U_{\infty}$$

2D Computational Studies

Angled Jet Validation Studies

- Left: LAVA Jet implementation matches OVERFLOW's normal blowing jet assumptions well.
- Right: Aero Coefficients consistent through angle sweep regardless of mass parameter used – introduced momentum is dominant effect on system.

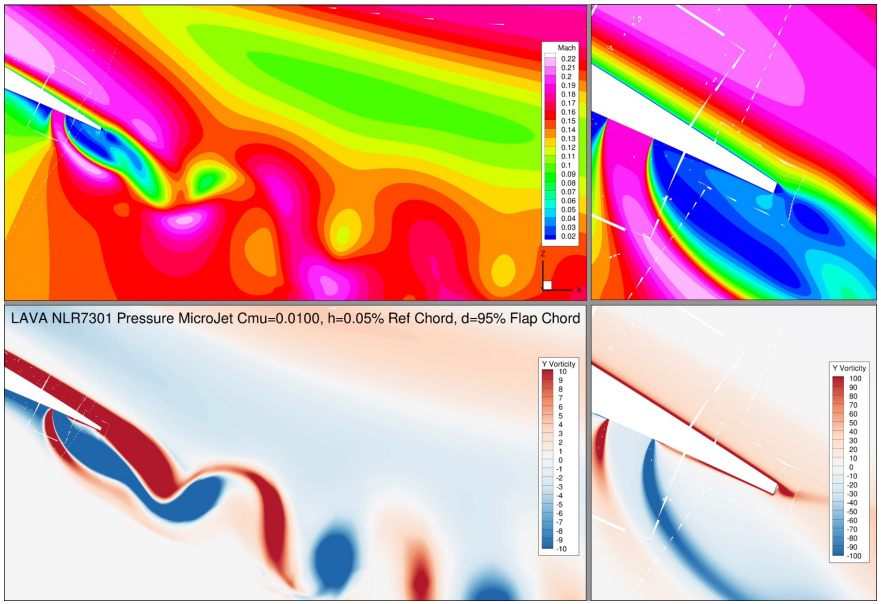


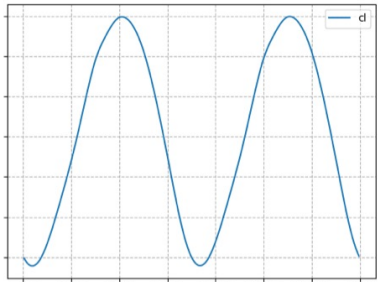


2D Computational Studies

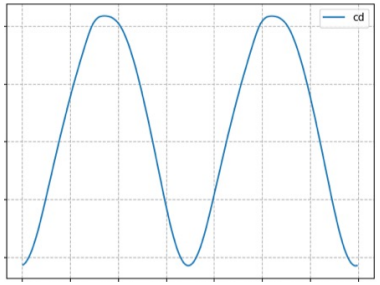
Normal Pressure-Side Jet Vortex Generation

$C_\mu = 0.01$



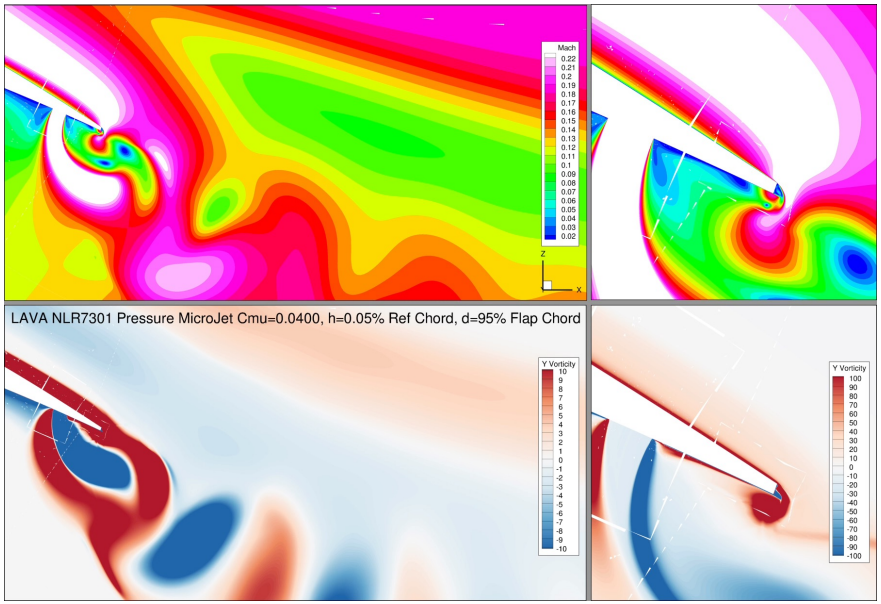


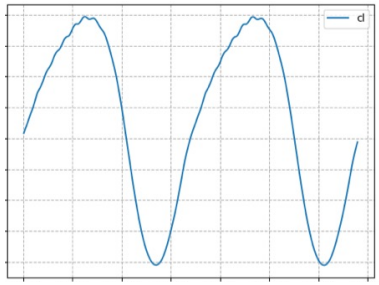
C_l



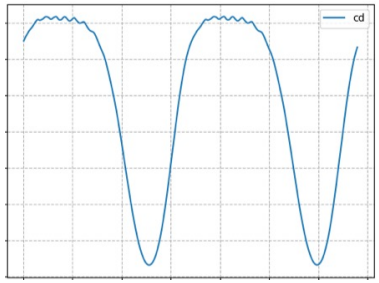
C_d

$C_\mu = 0.04$





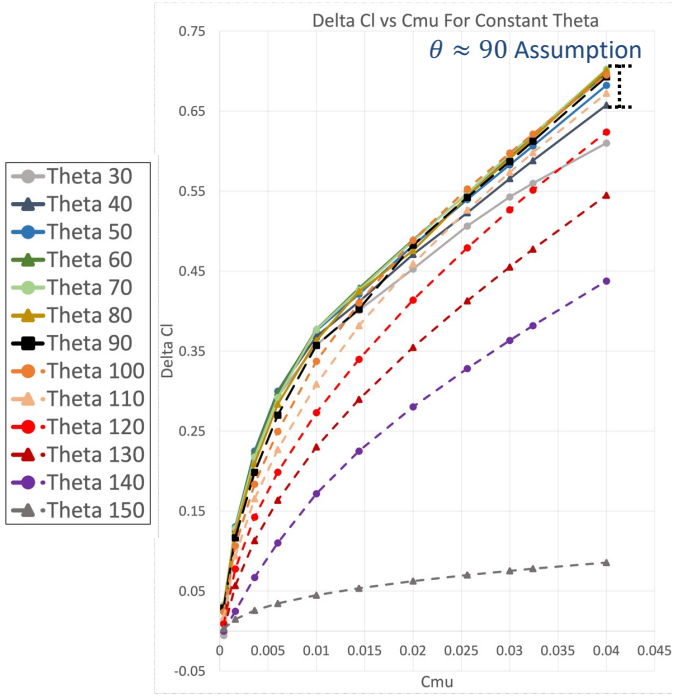
C_l



C_d

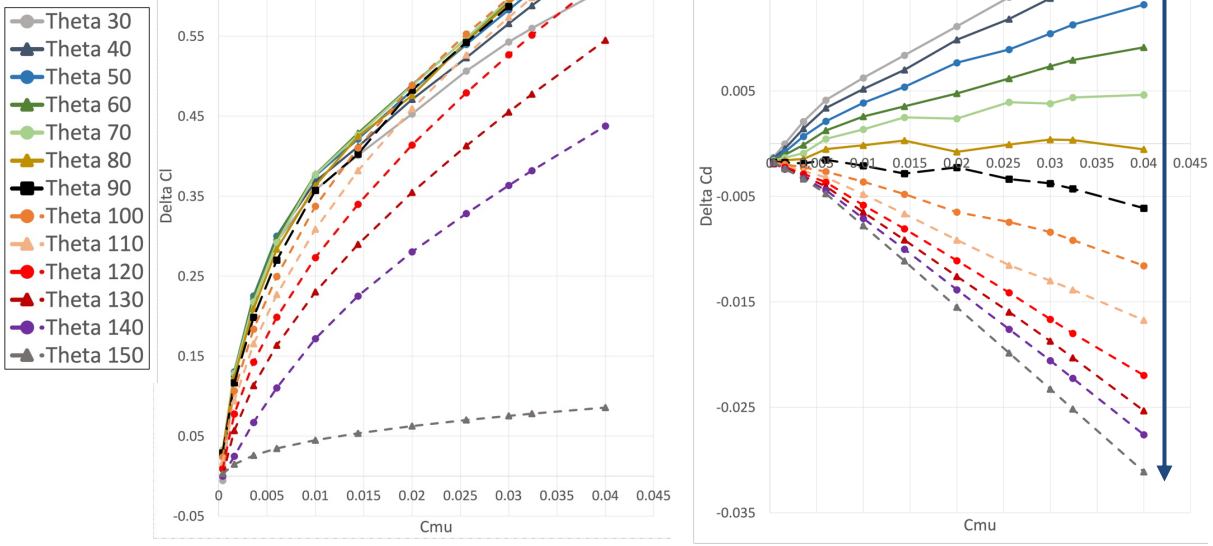
2D Computational Studies

Jet Angle Aero Trend Study (Constant θ)



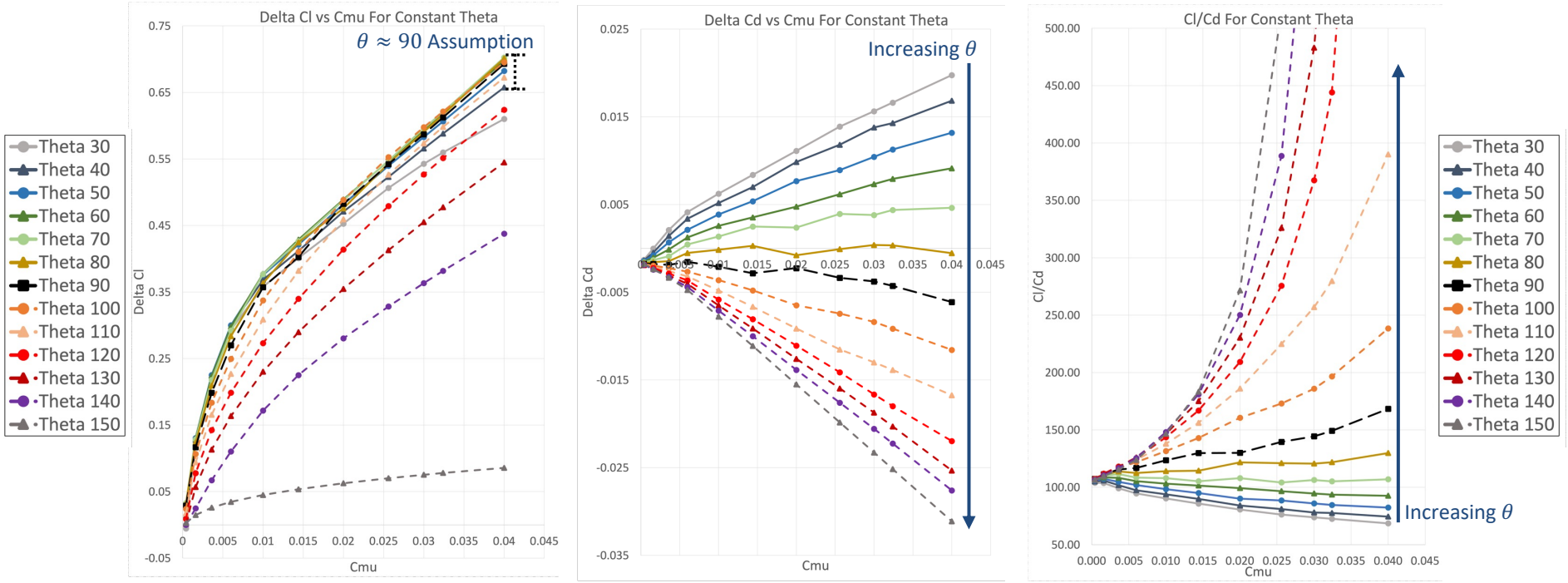
2D Computational Studies

Jet Angle Aero Trend Study (Constant θ)



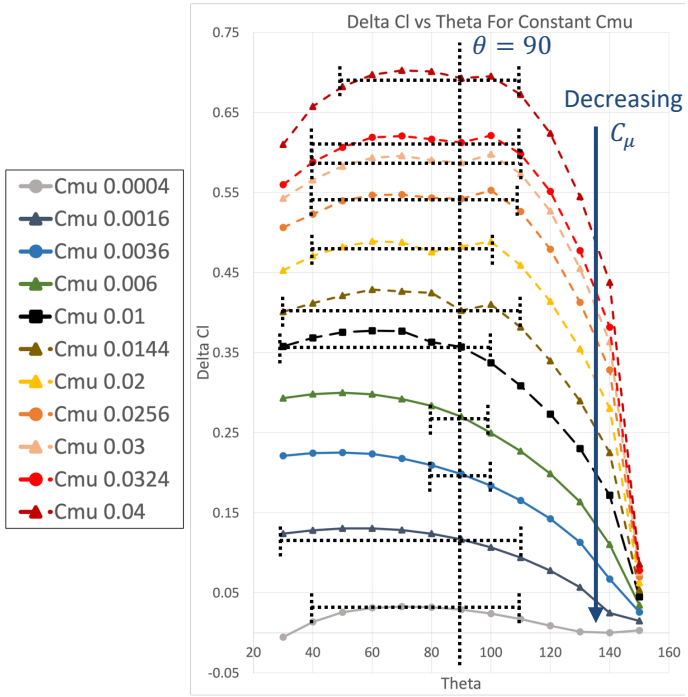
2D Computational Studies

Jet Angle Aero Trend Study (Constant θ)



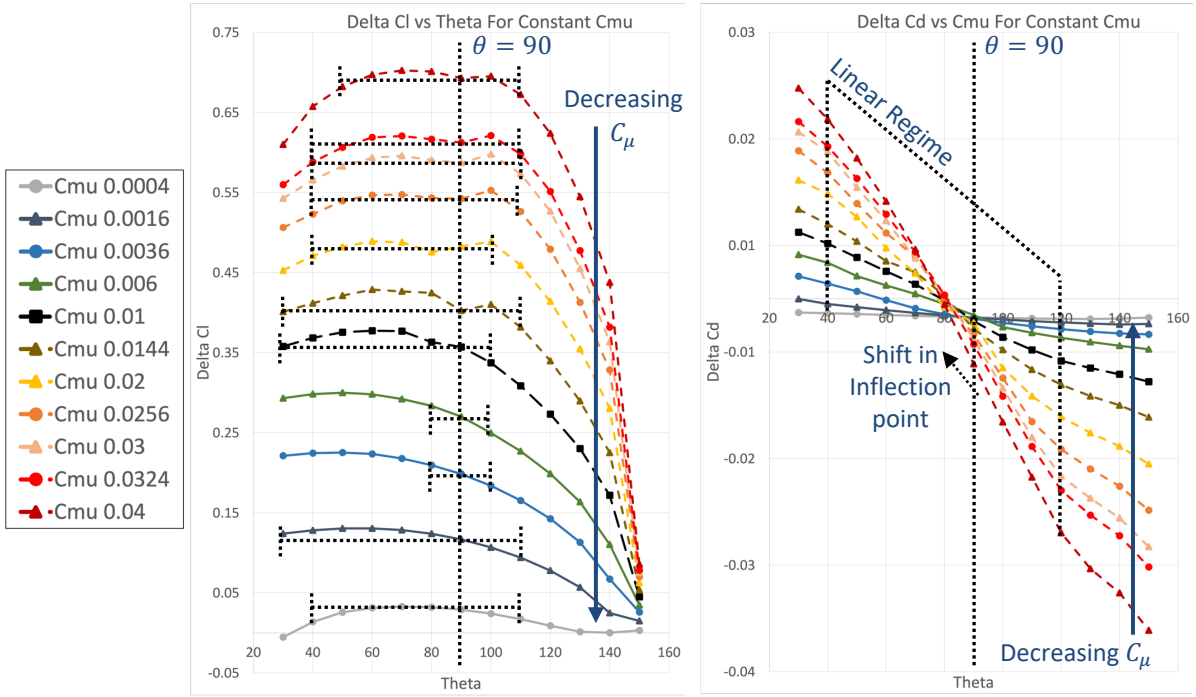
2D Computational Studies

Jet Angle Aero Trend Study (constant C_μ)



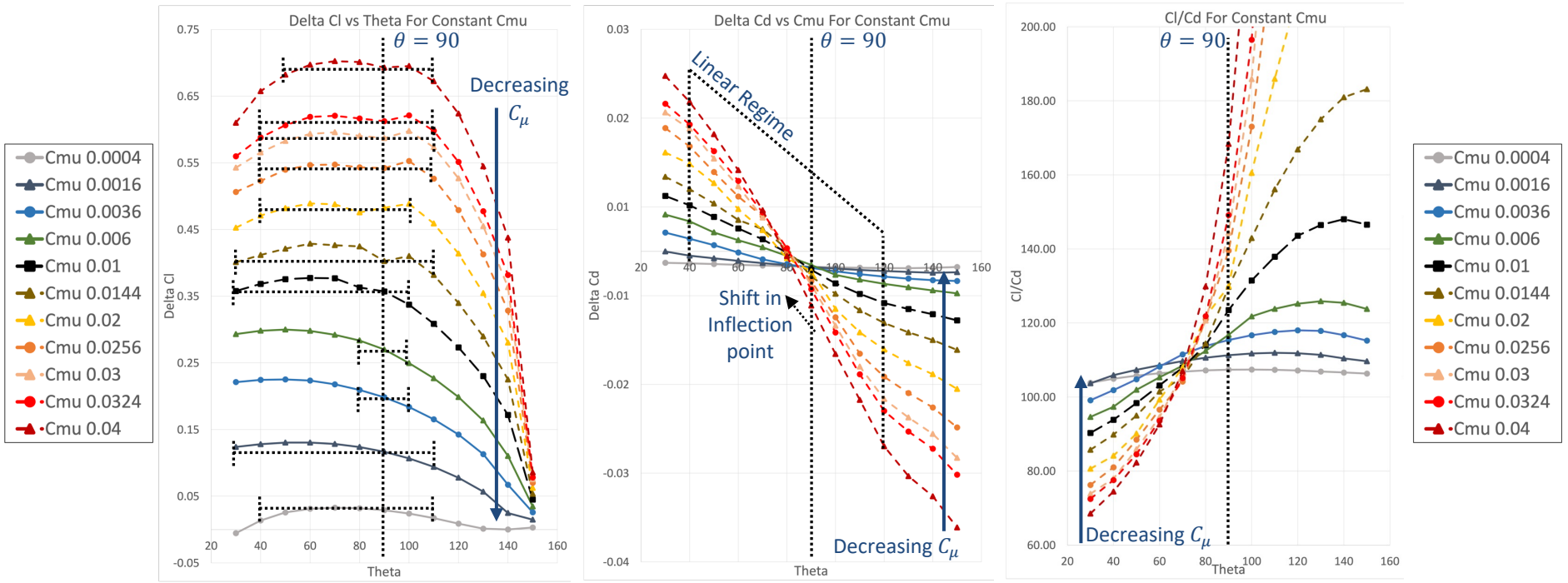
2D Computational Studies

Jet Angle Aero Trend Study (constant C_μ)



2D Computational Studies

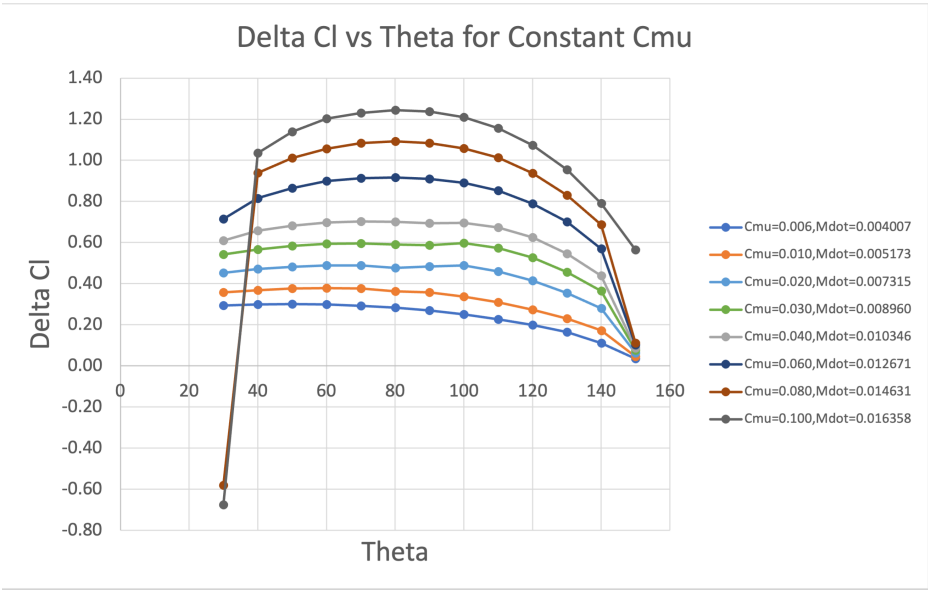
Jet Angle Aero Trend Study (constant C_μ)

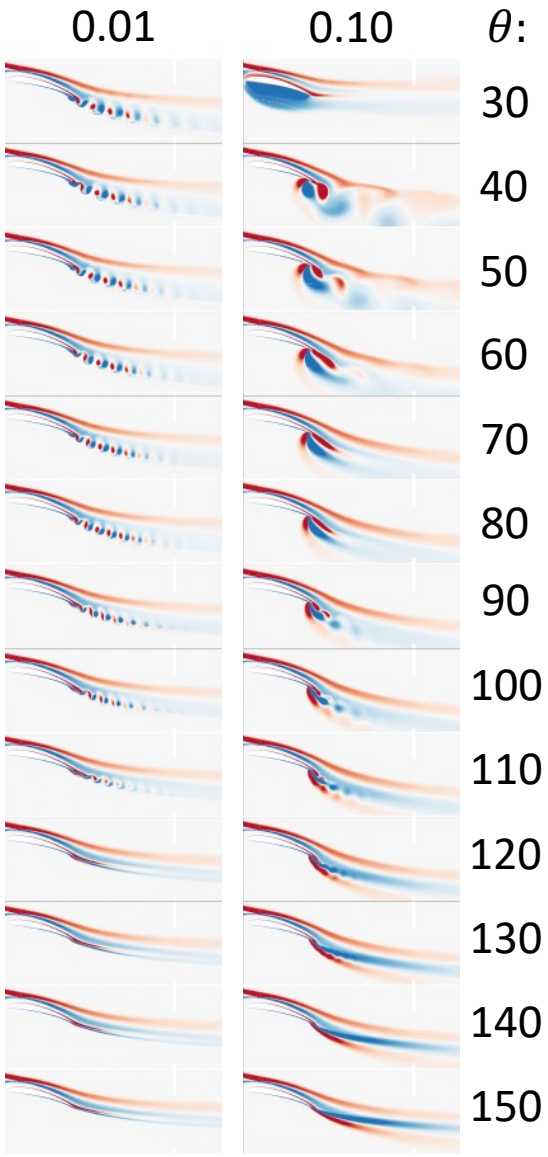


2D Computational Studies

Jet angle C_μ Flow Regime Study

- 'Application' C_μ is $\lesssim 0.02$, but explore C_μ up to 0.1.
- Trends seen at lower C_μ hold, but become more shifted/sloped at higher C_μ.
- Interesting steady 'locking' seen at high C_μ for upstream θ.
- Downstream (~tangent) θ leads to steady solutions.





Y Voritcity

2D Computational Studies

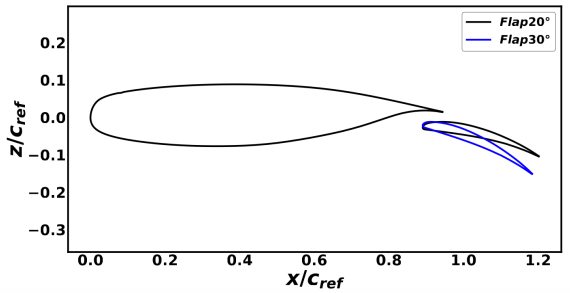
Jet Angle Lessons Learned

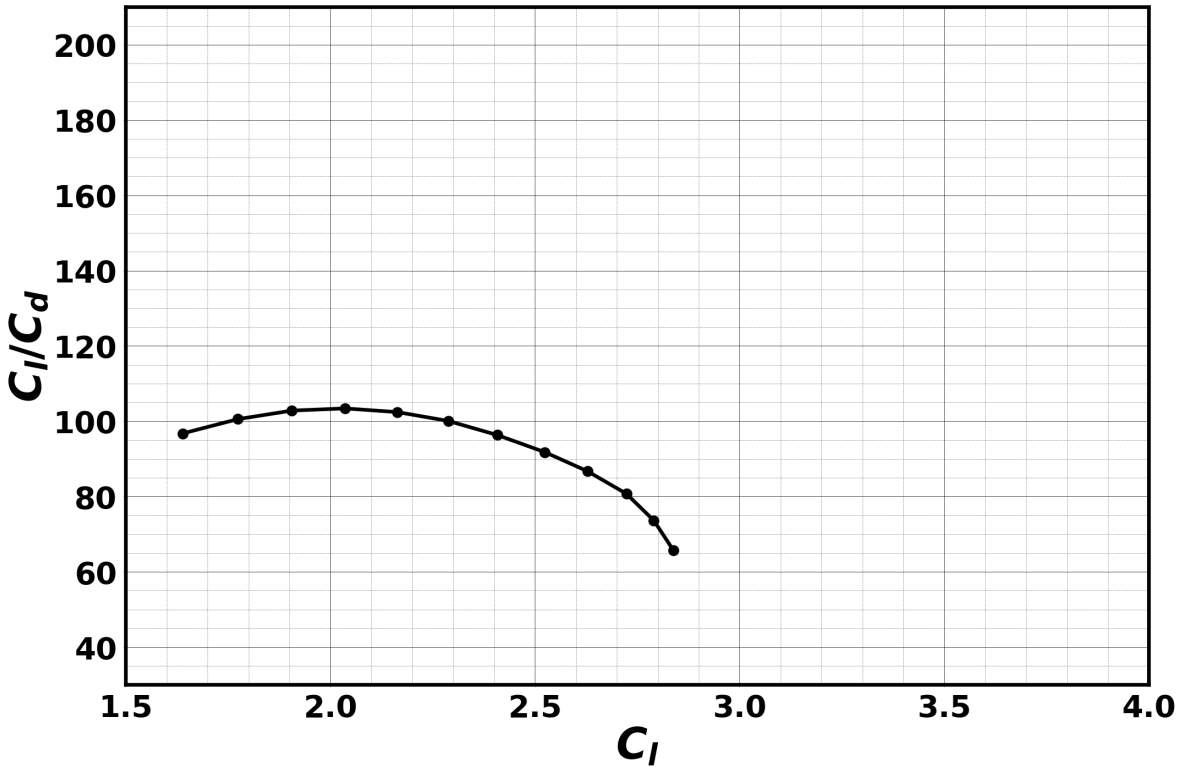
- For constant θ:
  - $\boldsymbol{\Delta C_l = K\sqrt{C_\mu}}$ **normal blowing assumption holds for** $\boldsymbol{40° \lessapprox \theta \lessapprox 110°}$.
  - $\boldsymbol{\Delta C_d}$ **follows linear trend, with slope clearly dependent on** $\boldsymbol{\theta}$ due to retro-propulsion/thrusting effects.
  - θ has clear exponential scaling effect on C_l/C_d for a given C_μ, which is unsurprising since higher θs decrease drag to near 0 due to thrusting effect.
- For constant C_μ:
  - **Normal blowing** $\boldsymbol{\Delta C_l}$ **holds for a** $\boldsymbol{C_\mu}$**-dependent range of** $\boldsymbol{\theta}$ **local to 90.**
  - ΔC_d has a decreasing linear regime from $40° \lessapprox \theta \lessapprox 120°$ with slope and inflection point dependent on C_μ. **Increasing** $\boldsymbol{C_\mu}$ **increases sensitivity of** $\boldsymbol{C_d}$ **to** $\boldsymbol{\theta}$.
  - C_μ has clear scaling and shifting effect on the sigmoidal C_l/C_d trends - especially when the jet is angled near tangential-blowing where trends at high C_μ turn nearly exponential.
- Exploration of 'unusual' jet strength and angle combinations should be integrated into testing of microjet technologies.

2D Computational Studies

Lift enhancement



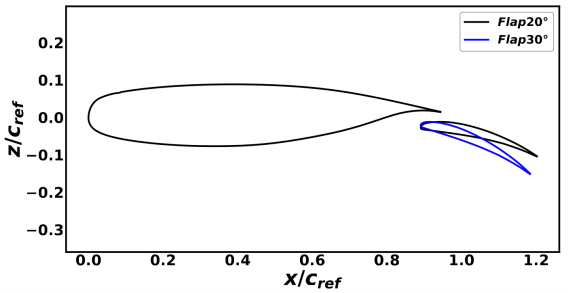




Hosseini, Seyedeh Sheida, et al. "Microjet Configuration Sensitivities for Active Flow Control on Multi-Element High-Lift Systems." *Journal of Aircraft* 58.4 (2021): 743-761

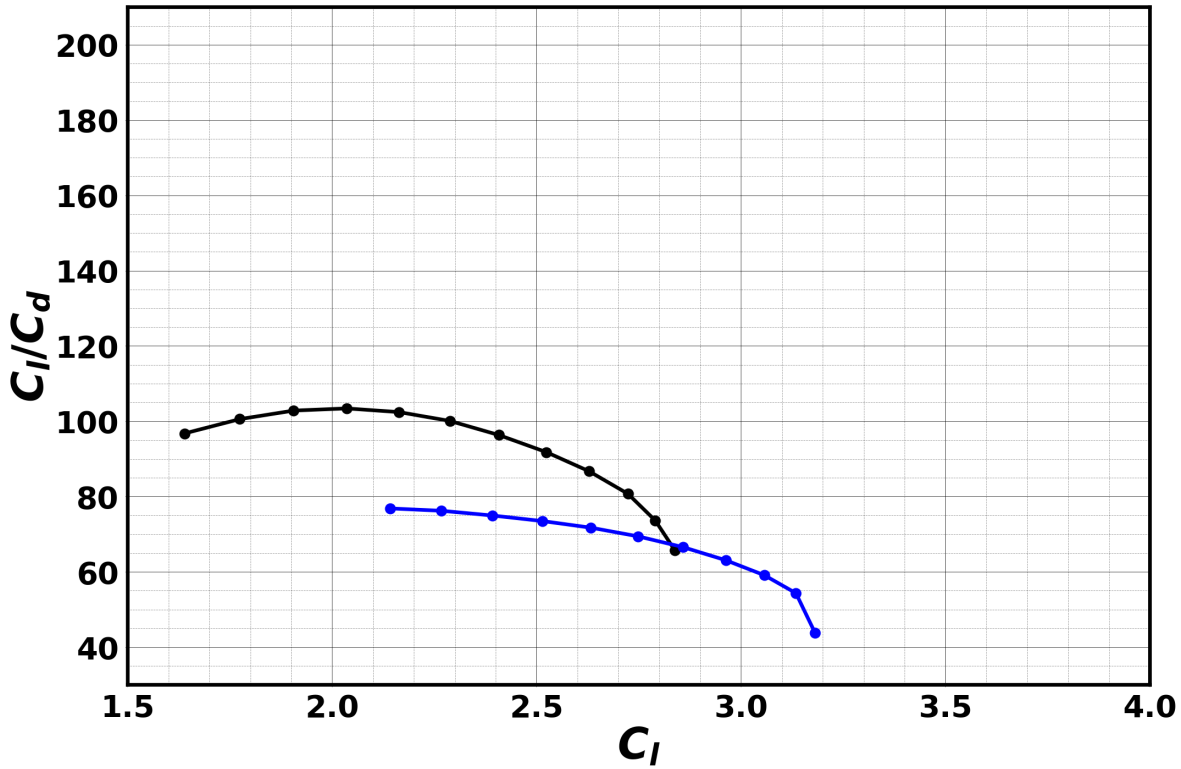
2D Computational Studies

Lift enhancement



Flap 20° Baseline (No Microjet), α Sweep

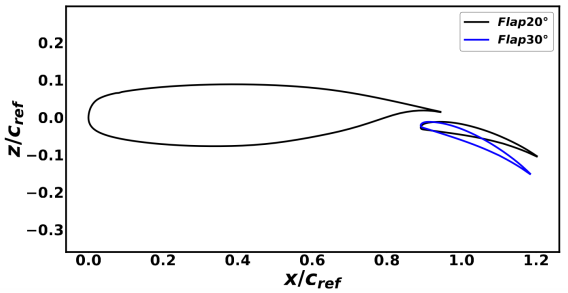
Flap 30° Baseline (No Microjet) α Sweep



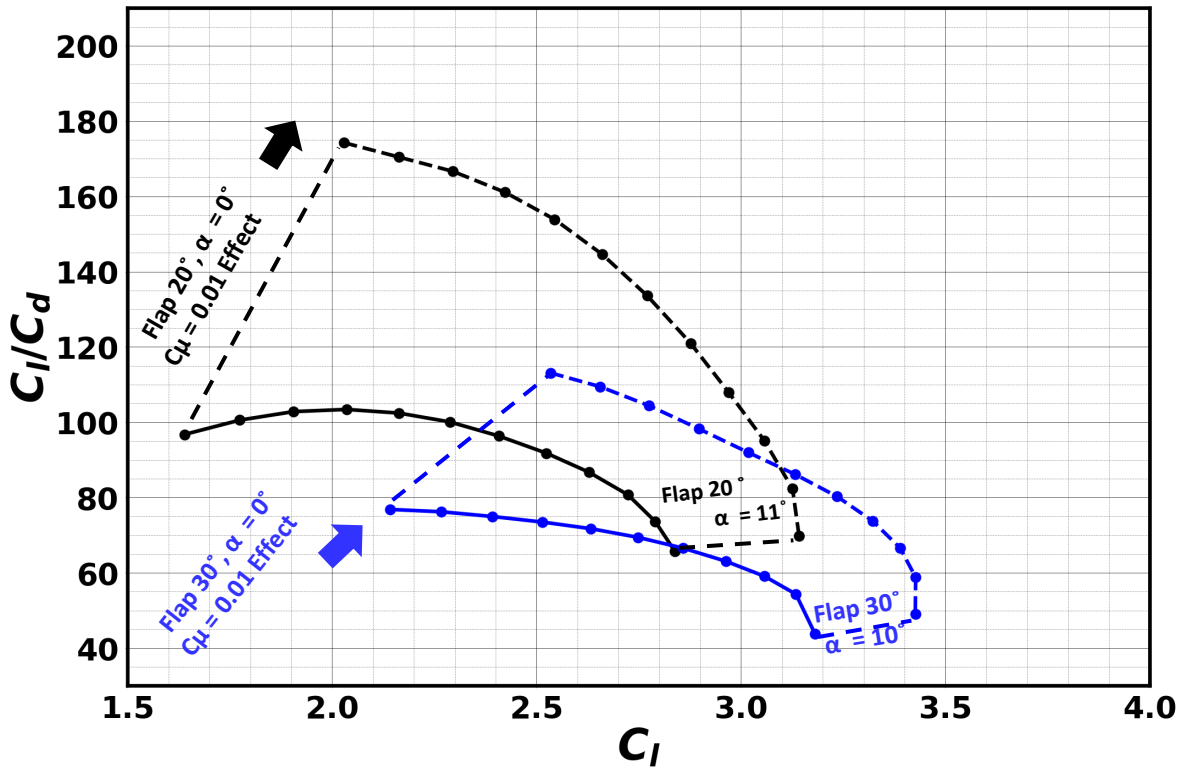
Hosseini, Seyedeh Sheida, et al. "Microjet Configuration Sensitivities for Active Flow Control on Multi-Element High-Lift Systems." *Journal of Aircraft* 58.4 (2021): 743-761

2D Computational Studies

Lift enhancement



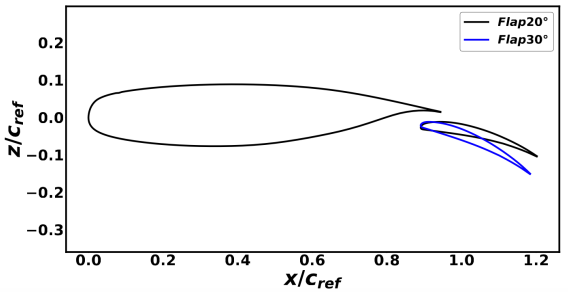
Flap 20° Baseline (No Microjet), α Sweep
Flap 20° Pressure-Side Microjet, Cμ = 0.01, α Sweep
Flap 30° Baseline (No Microjet) α Sweep
Flap 30° Pressure-Side Microjet Cμ = 0.01, α Sweep



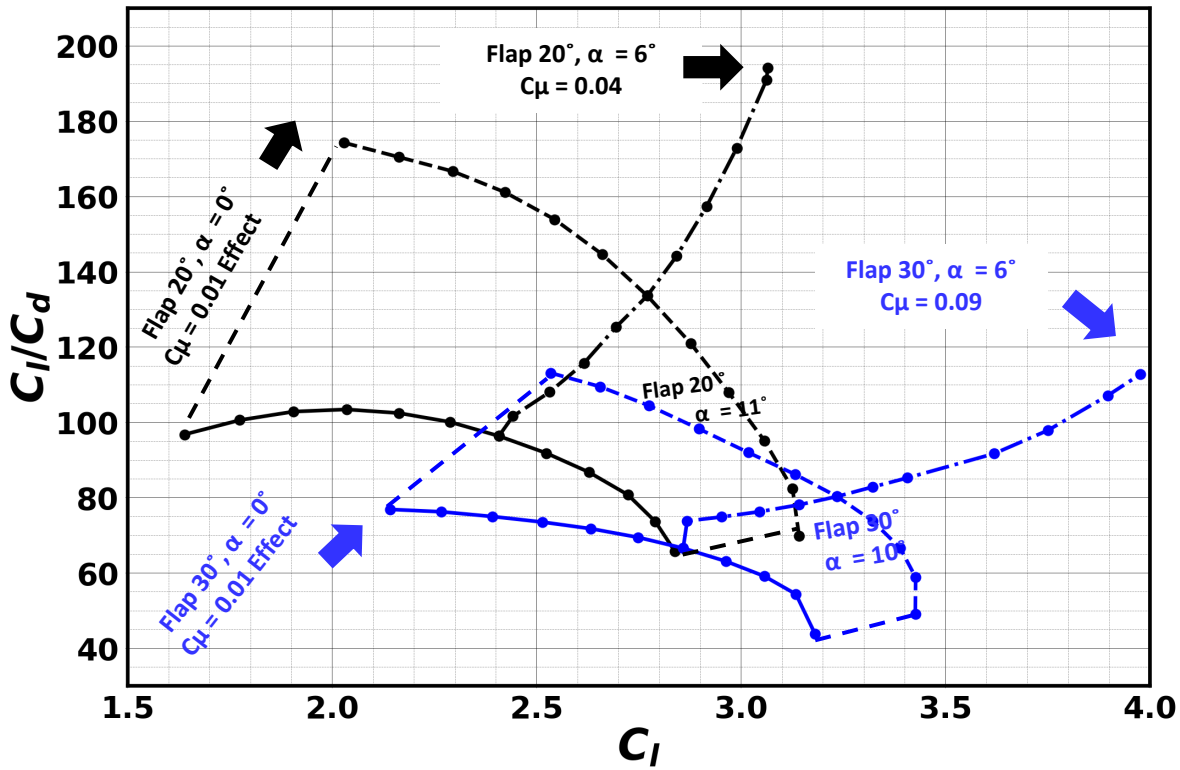
Hosseini, Seyedeh Sheida, et al. "Microjet Configuration Sensitivities for Active Flow Control on Multi-Element High-Lift Systems." *Journal of Aircraft* 58.4 (2021): 743-761

2D Computational Studies

Lift enhancement



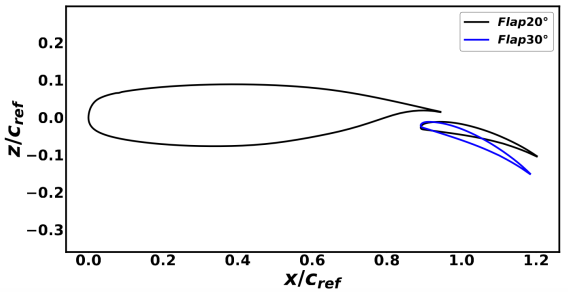
Flap 20° Baseline (No Microjet), α Sweep
Flap 20° Pressure-Side Microjet, Cμ = 0.01, α Sweep
Flap 20° Pressure-Side Microjet at α = 6°, Cμ Sweep
Flap 30° Baseline (No Microjet) α Sweep
Flap 30° Pressure-Side Microjet Cμ = 0.01, α Sweep
Flap 30° Pressure-Side Micorjet at α = 6°, Cμ Sweep



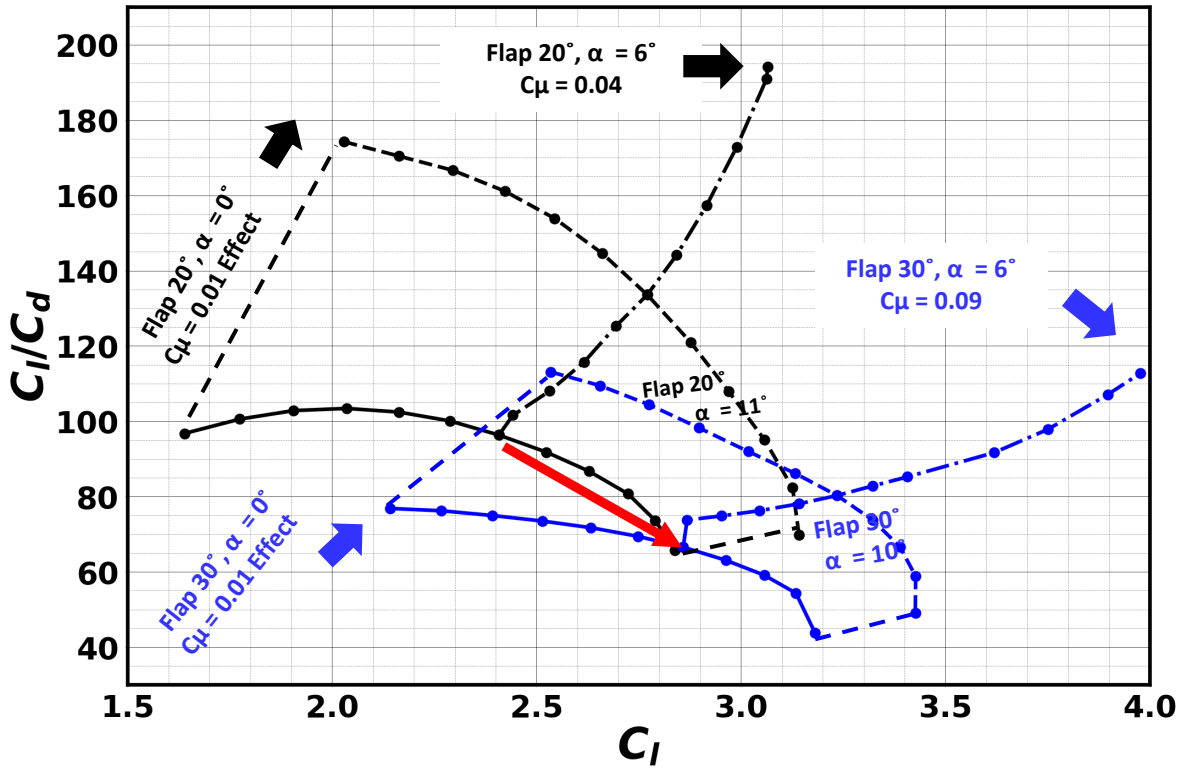
Hosseini, Seyedeh Sheida, et al. "Microjet Configuration Sensitivities for Active Flow Control on Multi-Element High-Lift Systems." *Journal of Aircraft* 58.4 (2021): 743-761

2D Computational Studies

Lift enhancement



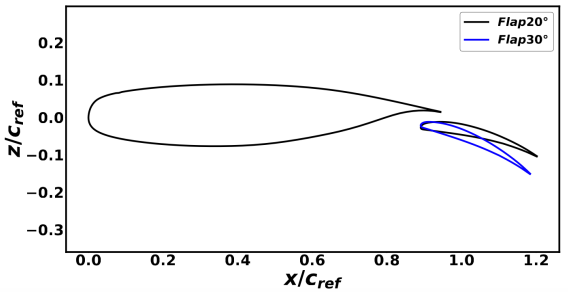
Flap 20° Baseline (No Microjet), α Sweep
Flap 20° Pressure-Side Microjet, Cμ = 0.01, α Sweep
Flap 20° Pressure-Side Microjet at α = 6°, Cμ Sweep
Flap 30° Baseline (No Microjet) α Sweep
Flap 30° Pressure-Side Microjet Cμ = 0.01, α Sweep
Flap 30° Pressure-Side Micorjet at α = 6°, Cμ Sweep



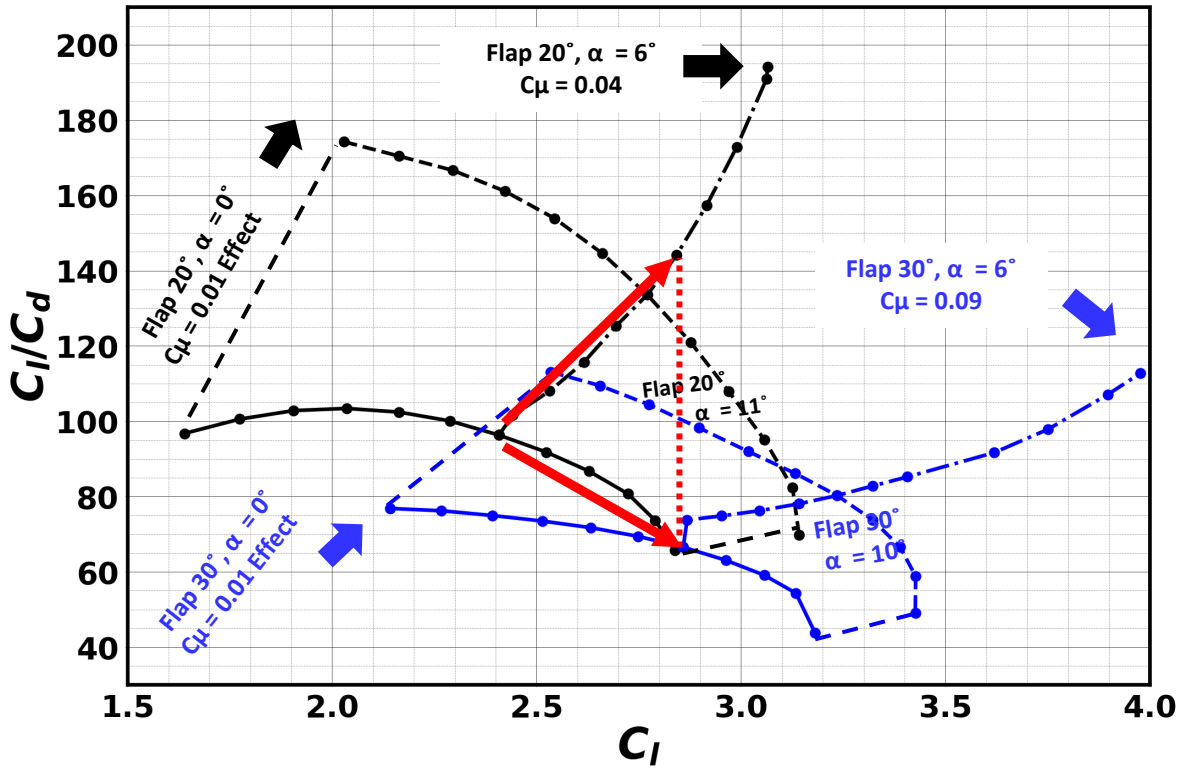
Hosseini, Seyedeh Sheida, et al. "Microjet Configuration Sensitivities for Active Flow Control on Multi-Element High-Lift Systems." *Journal of Aircraft* 58.4 (2021): 743-761

2D Computational Studies

Lift enhancement

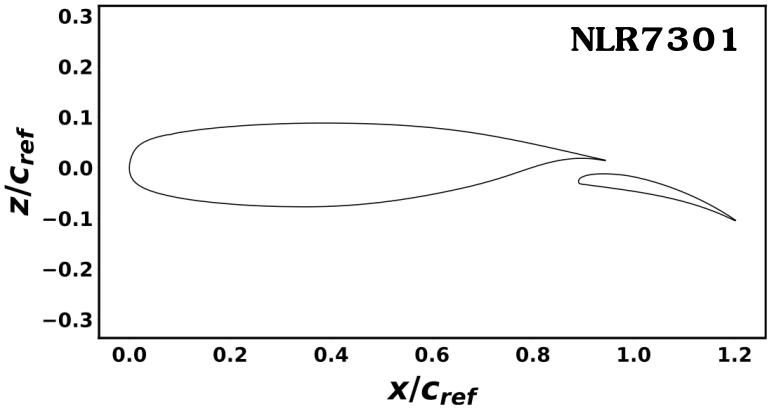


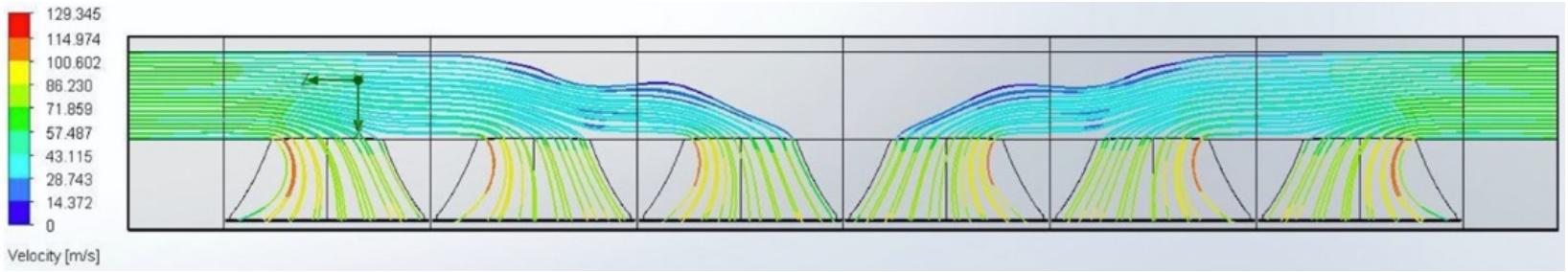
Flap 20° Baseline (No Microjet), α Sweep
Flap 20° Pressure-Side Microjet, Cμ = 0.01, α Sweep
Flap 20° Pressure-Side Microjet at α = 6°, Cμ Sweep
Flap 30° Baseline (No Microjet) α Sweep
Flap 30° Pressure-Side Microjet Cμ = 0.01, α Sweep
Flap 30° Pressure-Side Micorjet at α = 6°, Cμ Sweep



Hosseini, Seyedeh Sheida, et al. "Microjet Configuration Sensitivities for Active Flow Control on Multi-Element High-Lift Systems." *Journal of Aircraft* 58.4 (2021): 743-761

Summary of 2D experimental studies





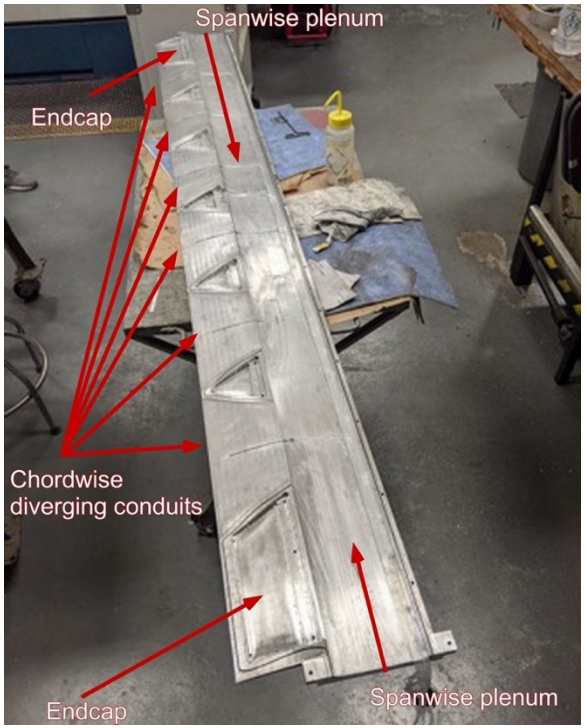
2D Wind Tunnel Studies

2D Wind Tunnel Test of Microjets

NLR-7301 two-element airfoil was tested in the 7 ft by 10 ft Oran W. Nicks Low-Speed Wind Tunnel at Texas A&M University

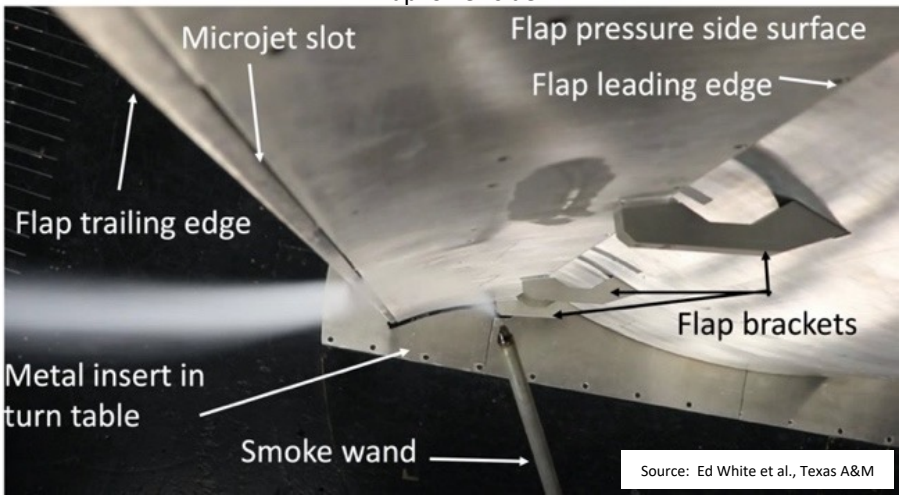
- Reynolds number = 2.0 million and Mach number = 0.10
- The wind tunnel results include surface pressure distributions, lift and pitching moment, and flow visualizations
- The results of this experiment validate the effectiveness of the microjet with regards to control of lift in the linear regime for multi-element airfoils
- Second wind tunnel entry in April 2023 to investigate details of microjet flow using Particle Image Velocimetry (PIV)

Flap lower-side panel depicting microjet flow paths



Source: Ed White et al., Texas A&M

Flap lower-side



van Dam, C. P., et al. "Wind Tunnel Experiment of Microjet-Based Flow Control on a Two-Dimensional Wing with Flap." *Journal of Aircraft* (2022): 1-4.

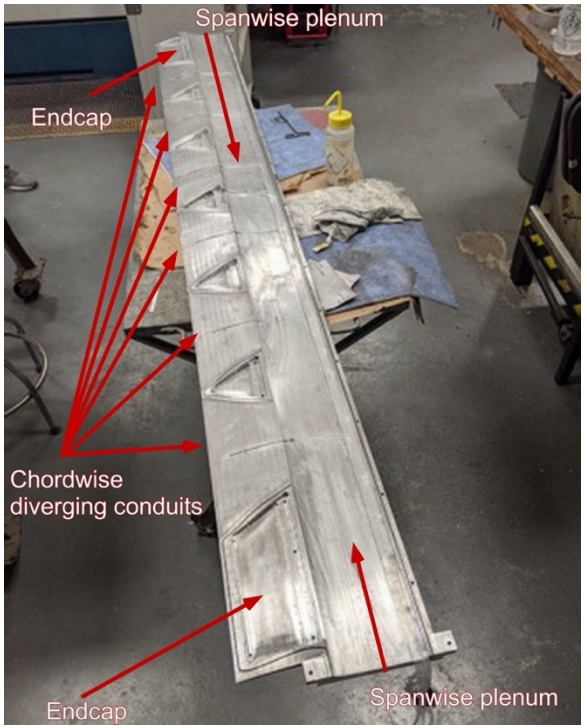
2D Wind Tunnel Studies

2D Wind Tunnel Test of Microjets

NLR-7301 two-element airfoil was tested in the 7 ft by 10 ft Oran W. Nicks Low-Speed Wind Tunnel at Texas A&M University

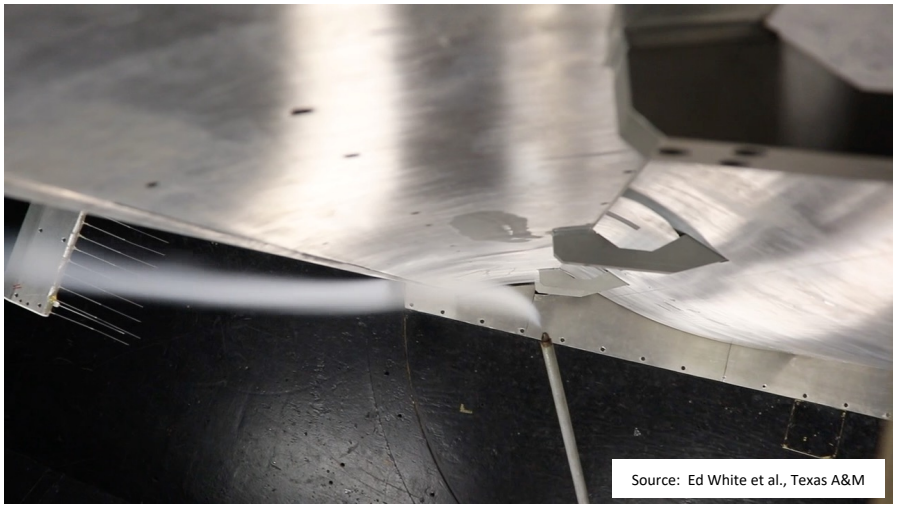
- Reynolds number = 2.0 million and Mach number = 0.10
- The wind tunnel results include surface pressure distributions, lift and pitching moment, and flow visualizations
- The results of this experiment validate the effectiveness of the microjet with regards to control of lift in the linear regime for multi-element airfoils
- Second wind tunnel entry in April 2023 to investigate details of microjet flow using Particle Image Velocimetry (PIV)

Flap lower-side panel depicting microjet flow paths



Source: Ed White et al., Texas A&M

Flap lower-side



van Dam, C. P., et al. "Wind Tunnel Experiment of Microjet-Based Flow Control on a Two-Dimensional Wing with Flap." *Journal of Aircraft* (2022): 1-4.

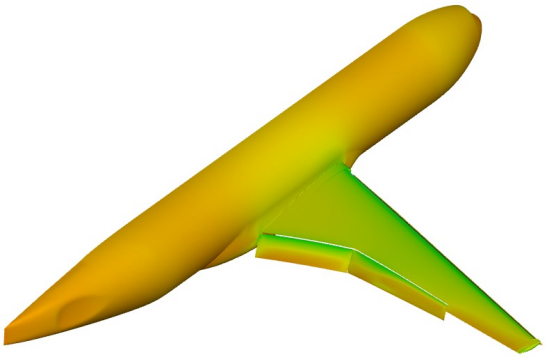
Summary of 3D computational studies

3D Computational Studies

HL-CRM is a wing-body configuration adapted for this study from HiLiftPW-3 Leading edge slats and trailing edge flaps deployed at 30˚ and 37˚, respectively

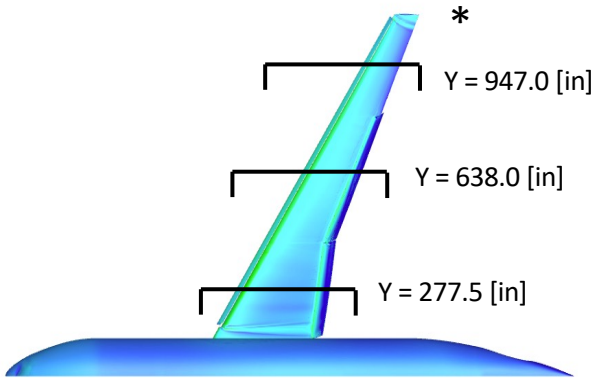
Not included in model:

- Flap and slat support brackets
- Pylon
- Nacelle
- Empennage



OVERFLOW Simulations:

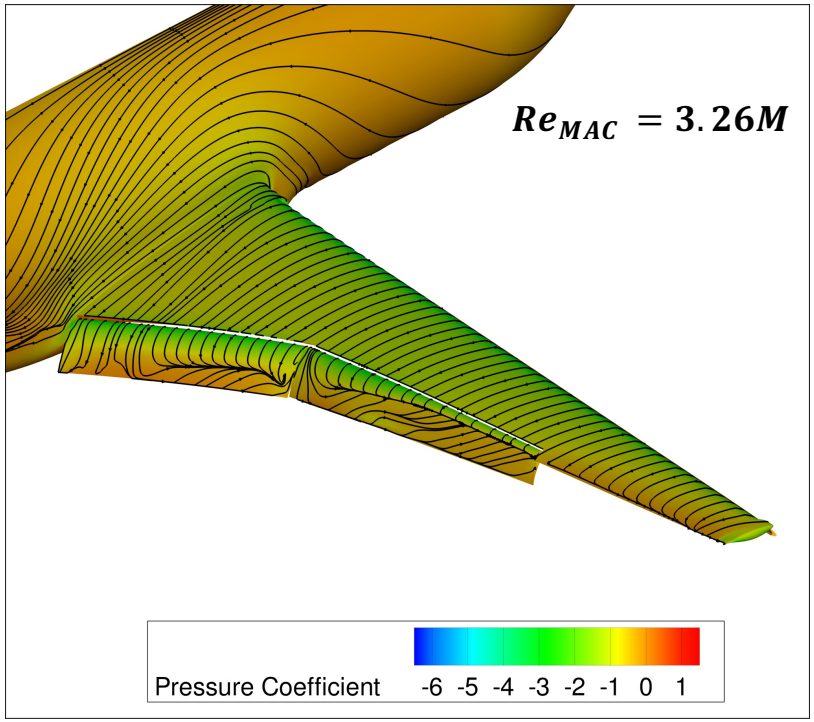
- Mach number = 0.2
- α = 8˚and AOA sweep
- Reynold MAC = 3.26M and 26.4M
  - MAC = 275.8 inches full scale
- Domain Connectivity Function routines
- Roe upwind scheme for spatial discretization
- F3D Steger-Warming 2-factor
- SA-RC-QCR2000 turbulence model
- RANS simulations on 432 Haswell cores



*Hosseini, Seyedeh Sheida, Case P. Van Dam, and Shishir Pandya. "Aerodynamic Assessment of Surface-Normal Active Flow Control for Lift Enhancement on the High-Lift Common Research Model." *AIAA SCITECH 2023 Forum*. 2023

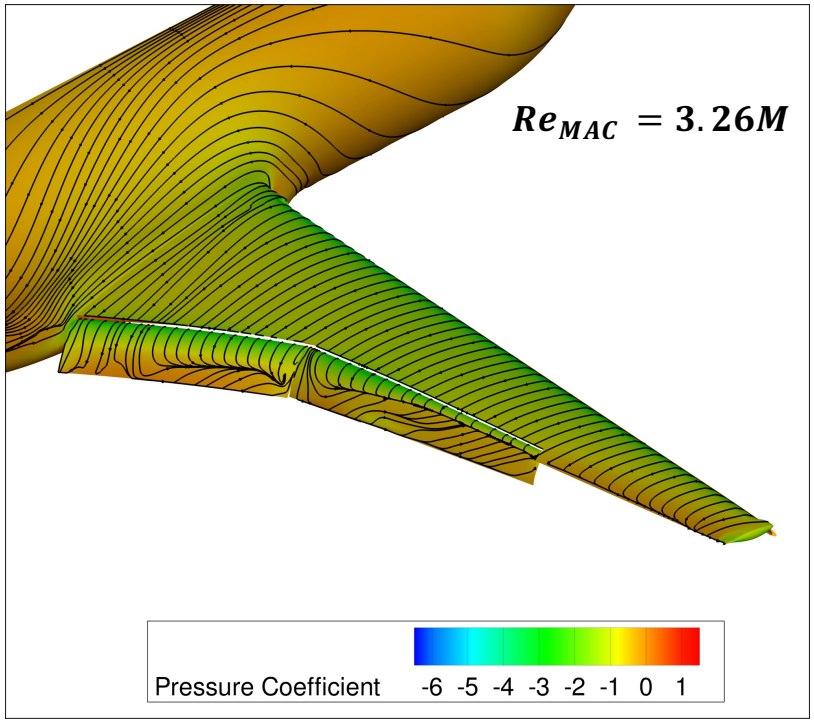
Microjet Effects on the Flow Features

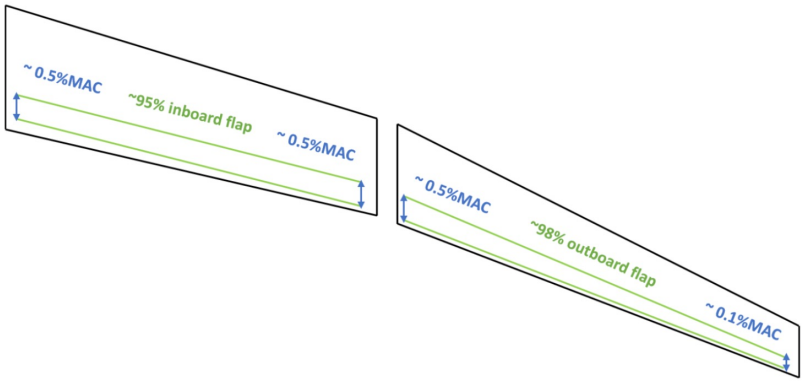
α=8°, Re_{MAC} = 3.26E6, and M = 0.2



Microjet Effects on the Flow Features

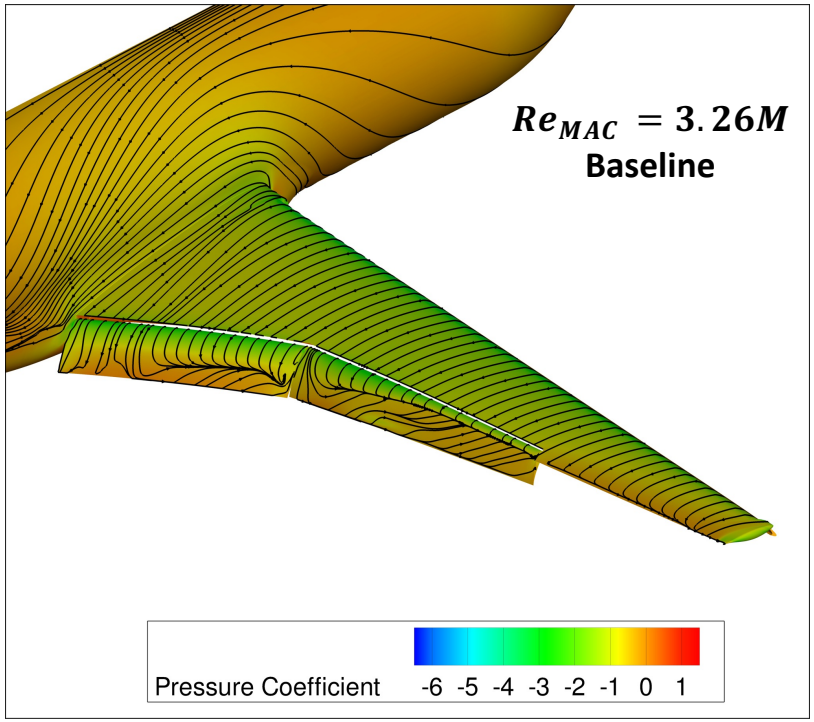
α=8°, Re_{MAC} = 3.26E6, and M = 0.2

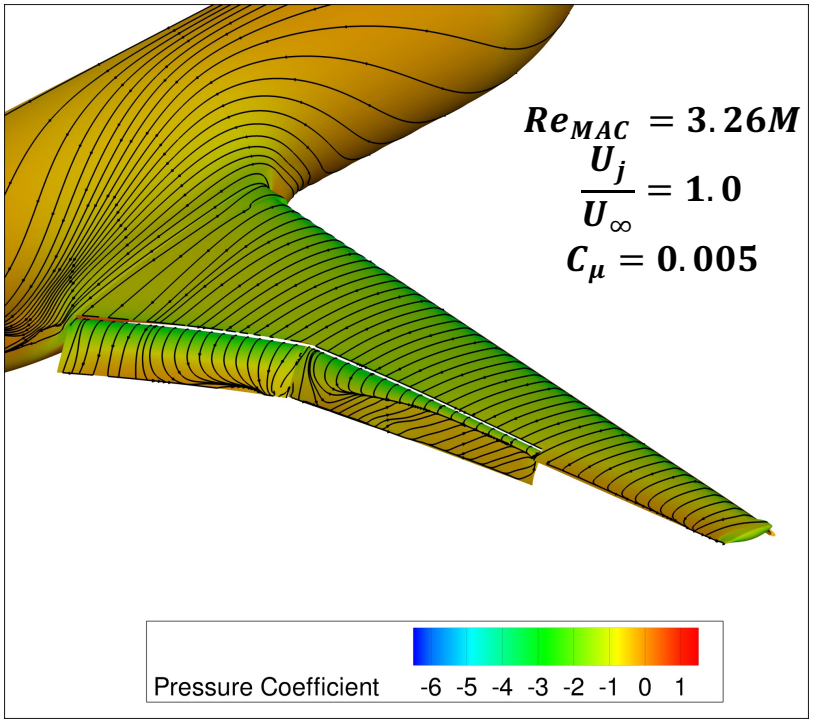




Microjet Effects on the Flow Features

α=8°, Re_{MAC} = 3.26E6, and M = 0.2

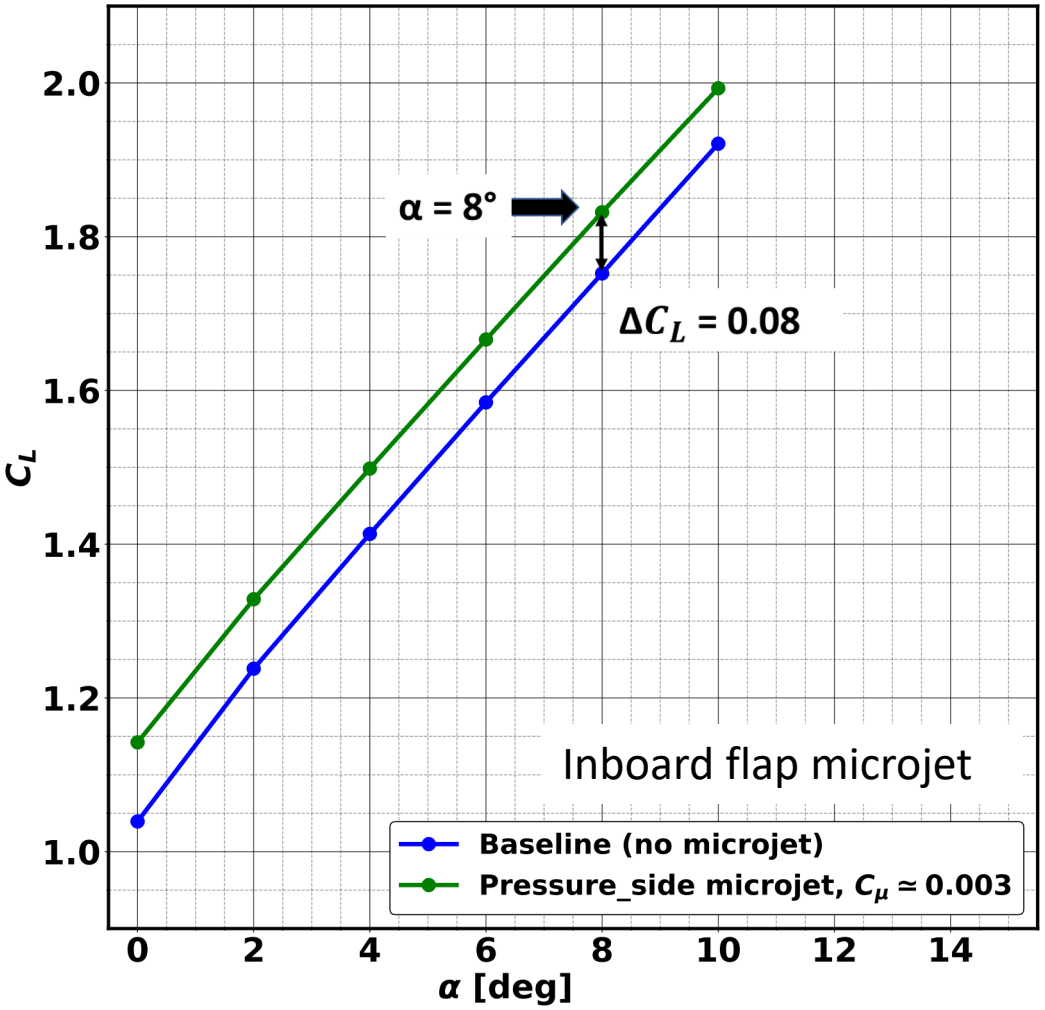




Configuration	Inboard and outboard flap microjet	Inboard Microjet	Outboard Microjet
ΔC_L	0.114	0.079	0.035

Microjet Effects on the Lift Curve

α=8°, Re_{MAC} = 3.26E6, and M = 0.2, U_j/U_∞ = 1.0

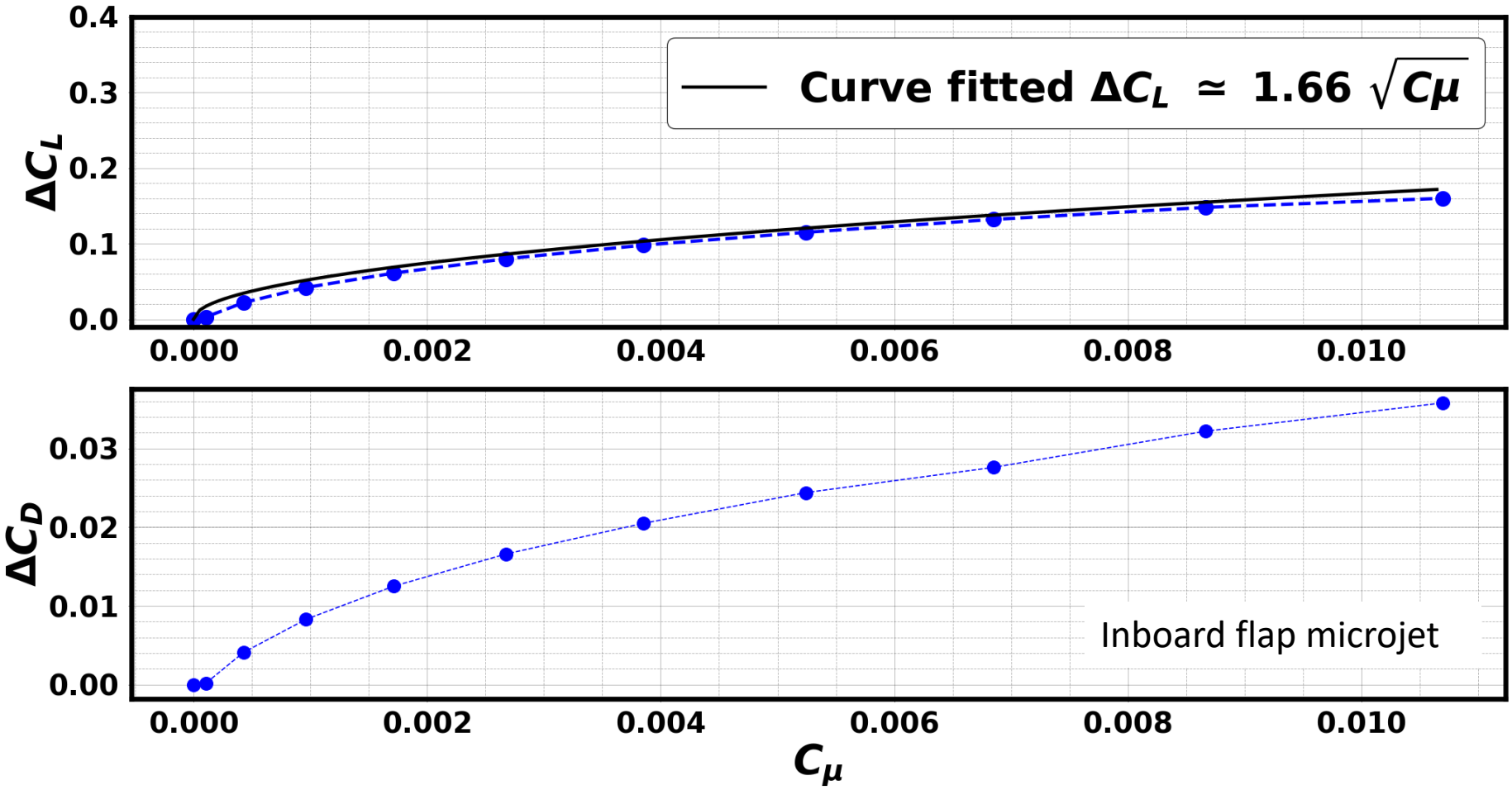


$\Delta C_L = 0.1$ can significantly impact landing gear selection and, hence, airplane empty weight.

*P. Meredith, "Viscous Phenomena Affecting High-Lift Systems and Suggestions for Future CFD Development. High-Lift System Aerodynamics," AGARD CP 515, pp. 19(1)–19(8), 1993.

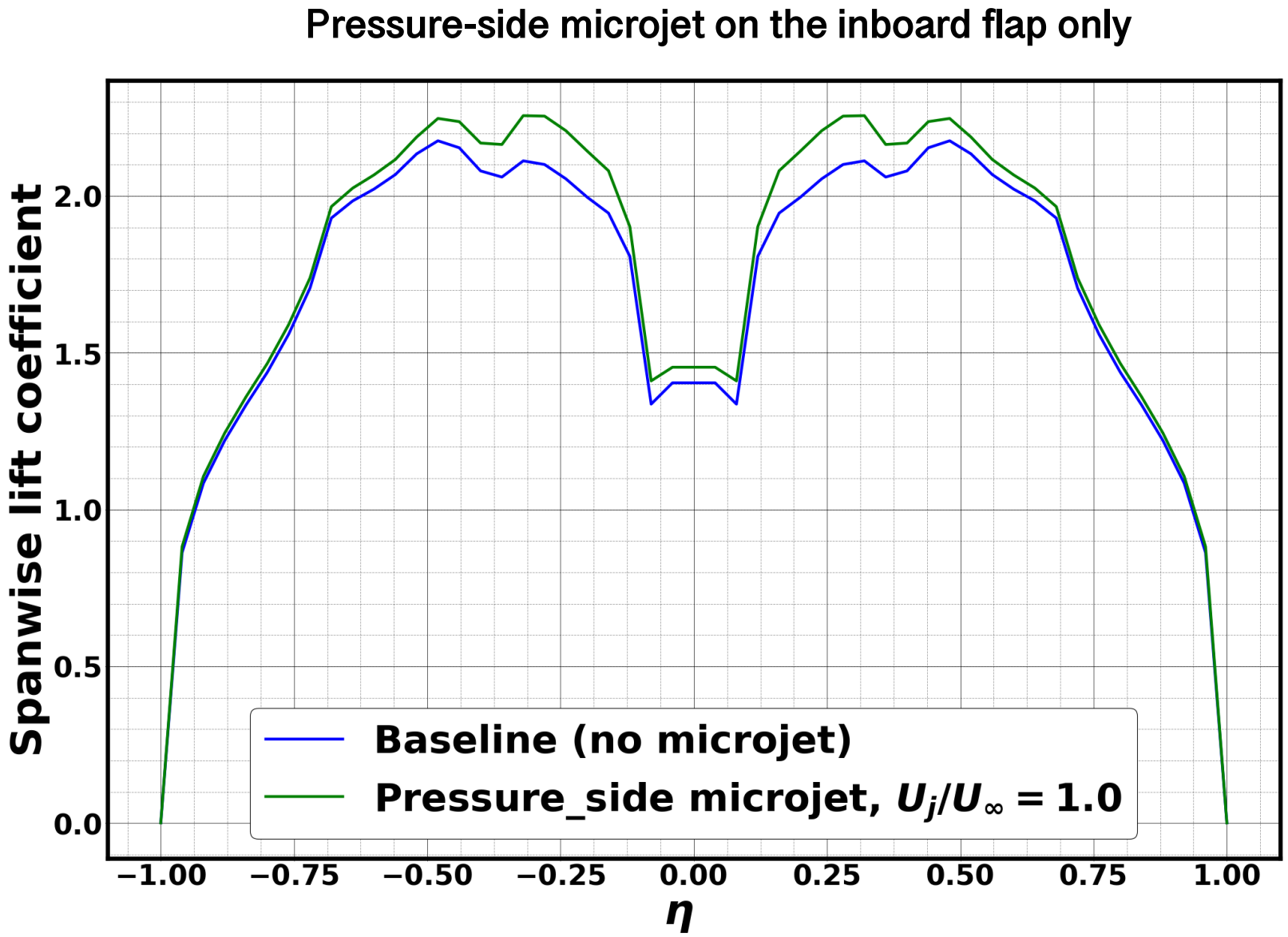
Microjet momentum Coefficient Effect

α=8°, Re_{MAC} = 3.26E6, and M = 0.2, U_j/U_∞ = 1.0



Hosseini, Seyedeh Sheida, Case P. Van Dam, and Shishir A. Pandya. "Surface-Normal Active Flow Control for Lift Enhancement and Separation Mitigation for High-Lift Common Research Model." *AIAA Scitech 2021 Forum*. 2021

Microjet Effect of the Spanwise Lift Distribution



Microjet Effect of the Drag Coefficient

Pressure integration	C_{L_p}	C_{D_p}	$C_{D_{p_{induced}}}$	$C_{D_{p_{form}}}$
Baseline (no microjet)	1.752	0.1508		
Pressure-side microjet on the inboard flap	1.830	0.1656		
Δ	0.078	0.0148		

$$\alpha_i(y_0) = \frac{1}{4\pi U_\infty} \int_{\frac{-b}{2}}^{\frac{b}{2}} \frac{d\Gamma}{dy} \frac{dy}{y_0 - y}$$

$$C_{D_i} = \frac{2}{U_\infty} \int_{\frac{-b}{2}}^{\frac{b}{2}} \Gamma(y)\alpha_i(y)dy$$

Hosseini, Seyedeh Sheida, Case P. Van Dam, and Shishir A. Pandya. "Surface-Normal Active Flow Control for Lift Enhancement and Separation Mitigation for High-Lift Common Research Model." *AIAA Scitech 2021 Forum*. 2021

Microjet Effect of the Drag Coefficient

Pressure integration	C_{L_p}	C_{D_p}	$C_{D_{p_{induced}}}$	$C_{D_{p_{form}}}$
Baseline (no microjet)	1.752	0.1508	0.1197	0.0311
Pressure-side microjet on the inboard flap	1.830	0.1656	0.1361	0.0295
Δ	0.078	0.0148	0.0164	-0.0016

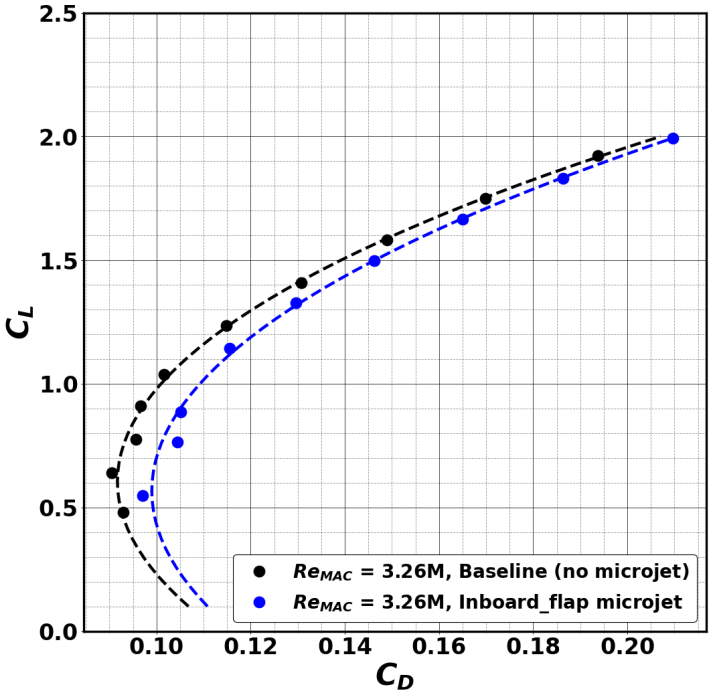
$$\alpha_i(y_0) = \frac{1}{4\pi U_\infty} \int_{\frac{-b}{2}}^{\frac{b}{2}} \frac{d\Gamma}{dy} \frac{dy}{y_0 - y}$$

$$C_{D_i} = \frac{2}{U_\infty} \int_{\frac{-b}{2}}^{\frac{b}{2}} \Gamma(y)\alpha_i(y)dy$$

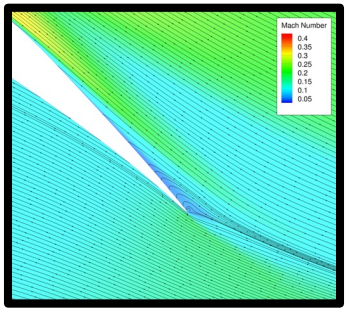
Hosseini, Seyedeh Sheida, Case P. Van Dam, and Shishir A. Pandya. "Surface-Normal Active Flow Control for Lift Enhancement and Separation Mitigation for High-Lift Common Research Model." *AIAA Scitech 2021 Forum*. 2021

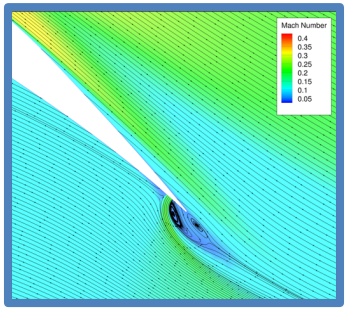
Wing Efficiency Assessment

$$C_D = C_{D_{min}} + \frac{(C_L - C_{L_{min}})^2}{\pi e AR} = (C_{D_{min}} + \frac{{C_{L_{min}}}^2}{\pi e AR}) + (\frac{-2C_{L_{min}}}{\pi e AR})C_L + (\frac{1}{\pi e AR}){C_L}^2$$



Configuration	Oswald Efficiency e	Δe
Baseline	%59.7	-
Inboard flap pressure microjet	%65.1	**%5.4**



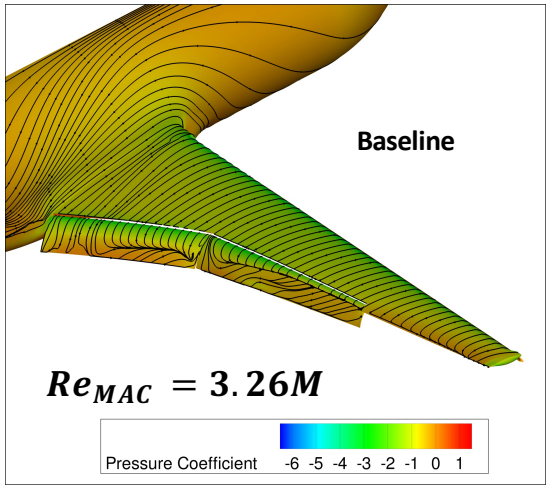


Microjet implemented for lift enhancement increases wing efficiency

Inboard flap microjet $\frac{U_j}{U_\infty} = 1.0$ and $C_\mu = 0.003$

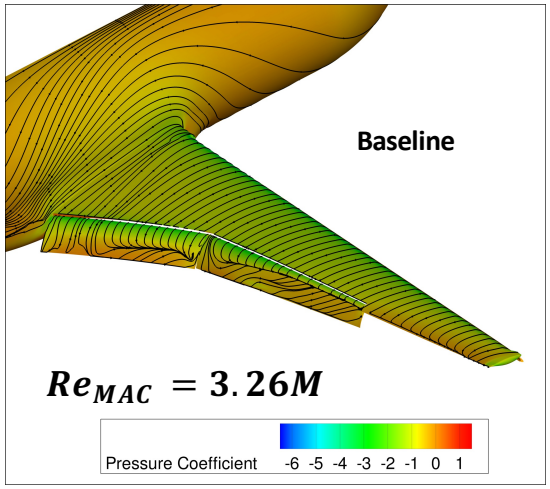
*Hosseini, Seyedeh Sheida, Case P. Van Dam, and Shishir Pandya. "Aerodynamic Assessment of Surface-Normal Active Flow Control for Lift Enhancement on the High-Lift Common Research Model." *AIAA SCITECH 2023 Forum*. 2023

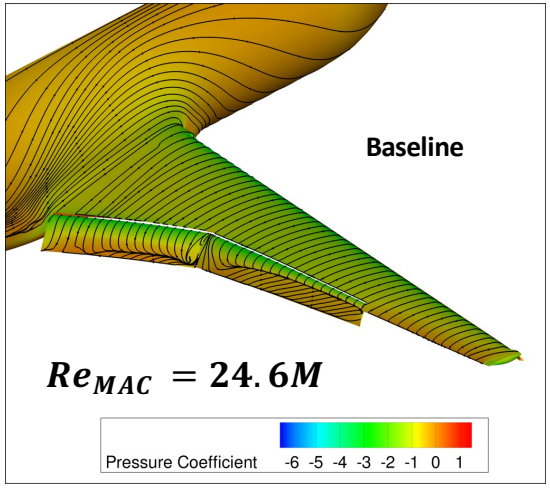
Reynolds Number Effects



*Hosseini, Seyedeh Sheida, Case P. Van Dam, and Shishir Pandya. "Aerodynamic Assessment of Surface-Normal Active Flow Control for Lift Enhancement on the High-Lift Common Research Model." *AIAA SCITECH 2023 Forum*. 2023

Reynolds Number Effects

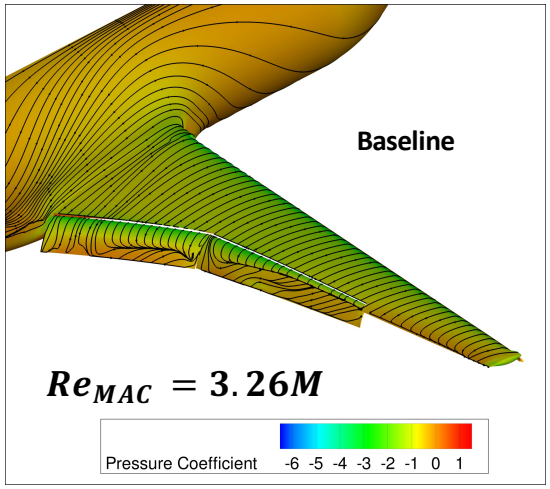


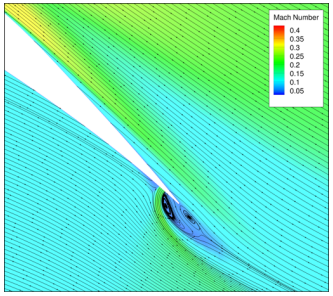


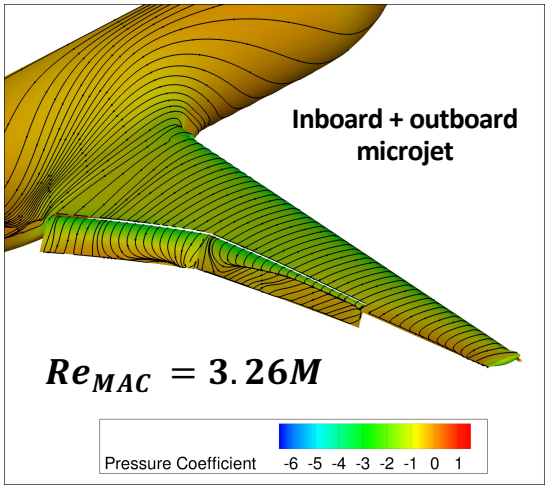
*Hosseini, Seyedeh Sheida, Case P. Van Dam, and Shishir Pandya. "Aerodynamic Assessment of Surface-Normal Active Flow Control for Lift Enhancement on the High-Lift Common Research Model." *AIAA SCITECH 2023 Forum*. 2023

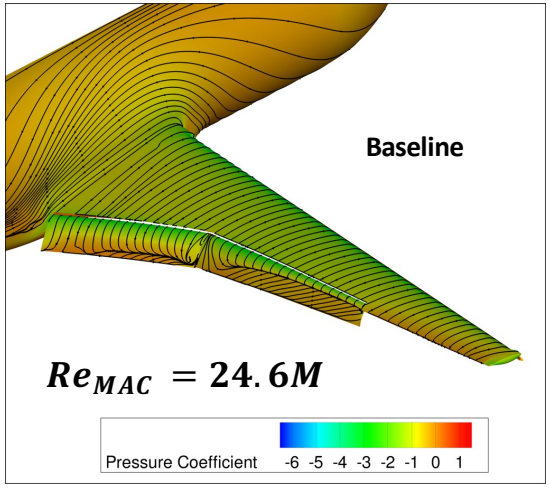
Reynolds Number Effects

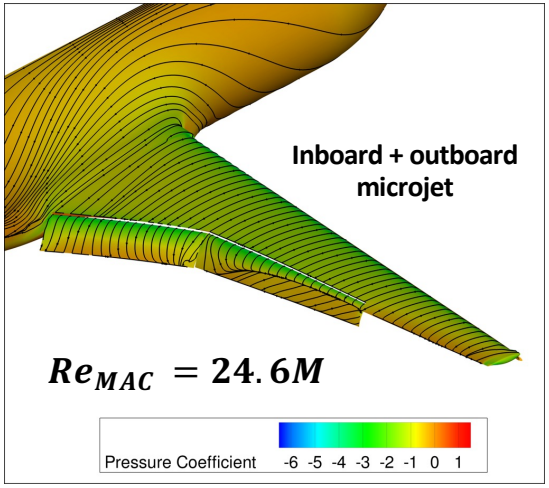
Microjets across both flaps on the lower surface at 95% flap chord with jet velocity ratio of unity.







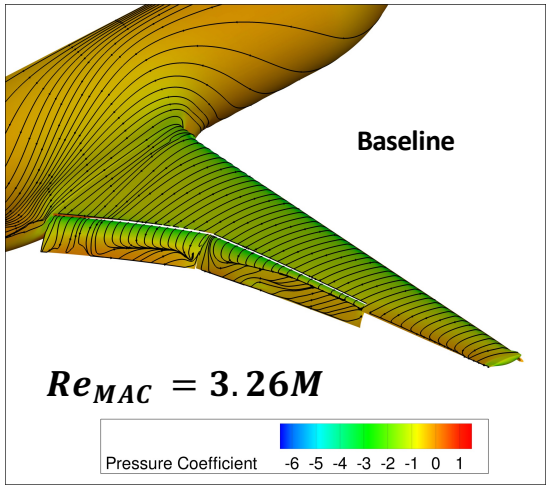


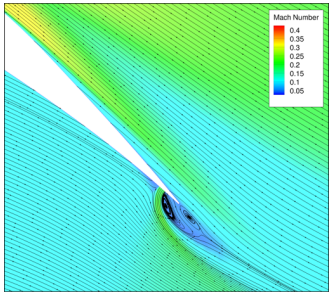


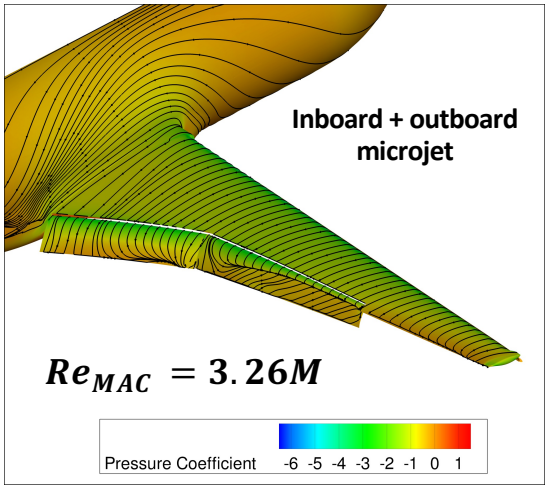
*Hosseini, Seyedeh Sheida, Case P. Van Dam, and Shishir Pandya. "Aerodynamic Assessment of Surface-Normal Active Flow Control for Lift Enhancement on the High-Lift Common Research Model." *AIAA SCITECH 2023 Forum*. 2023

Reynolds Number Effects

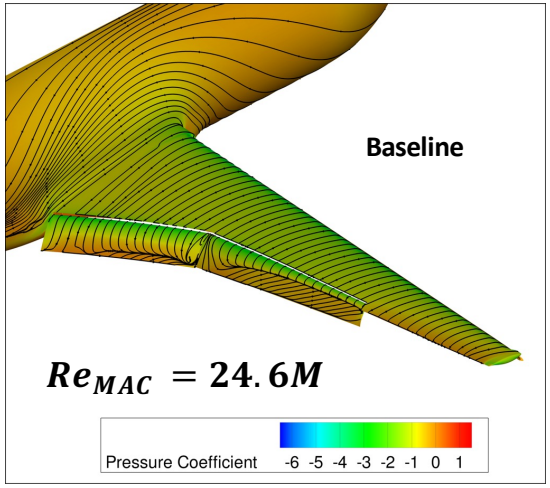
Microjets across both flaps on the lower surface at 95% flap chord with jet velocity ratio of unity.

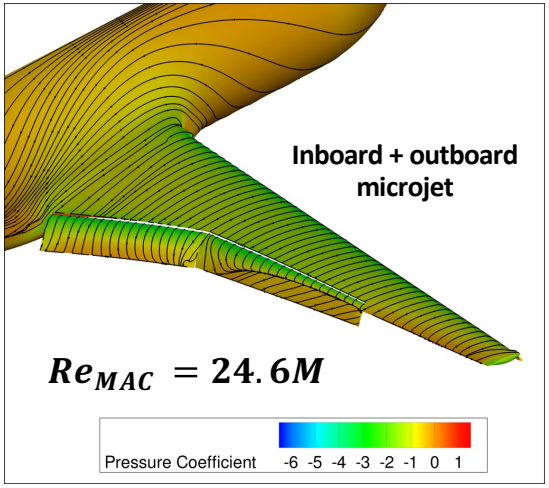






$\alpha = 8.0°$, M = 0.2	Δ C_L
RE $_{MAC}$ = 3.26E6	0.114
RE $_{MAC}$ = 24.6E6	0.120





Microjet trends on lift, drag, and Oswald efficiency are consistent at both Reynolds numbers.

*Hosseini, Seyedeh Sheida, Case P. Van Dam, and Shishir Pandya. "Aerodynamic Assessment of Surface-Normal Active Flow Control for Lift Enhancement on the High-Lift Common Research Model." *AIAA SCITECH 2023 Forum*. 2023

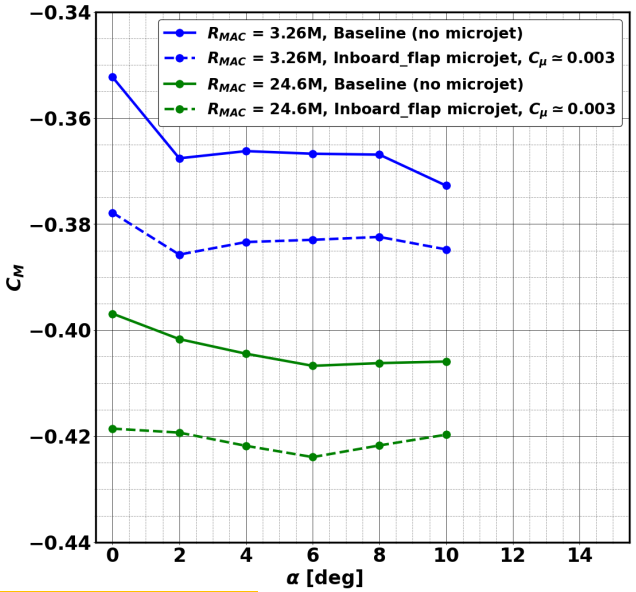
Microjet Effect on Trim Drag

Inboard flap microjet $\frac{U_j}{U_\infty} = 1.0$ and $C_\mu = 0.003$

Lift coefficients required by the horizontal tail to offset the pitching moment effects are supplied to the drag polars for trim drag estimates

$$C_{L_{trim}} = C_{L_{tailoff}} + C_{M_{tailoff}} \frac{MAC}{cos(\alpha)(X_{tail-MAC} - X_{cg}) + sin(\alpha)(Z_{tail-MAC} - Z_{cg})}$$

$\alpha = 8.0°$ and M = 0.2	$C_{D_{pre-trim}}$	$C_{D_{trim}}$	$C_{D_{total}}$	$\Delta C_{D_{trim}}$
$Re_{MAC} = 24.6 \times 10^6$				
Baseline	0.1706	0.0173	0.1879	-
Inboard-flap microjet	0.1874	0.0186	0.2060	0.0013
$Re_{MAC} = 3.26 \times 10^6$				
Baseline	0.1698	0.0153	0.1851	-
Inboard-flap microjet	0.1864	0.0161	0.2025	0.0008



Microjet implemented for lift enhancement increases trim drag by ~ 0.5% total drag

*Hosseini, Seyedeh Sheida, Case P. Van Dam, and Shishir Pandya. "Aerodynamic Assessment of Surface-Normal Active Flow Control for Lift Enhancement on the High-Lift Common Research Model." *AIAA SCITECH 2023 Forum*. 2023

Microjet Load Control Capability

Problem

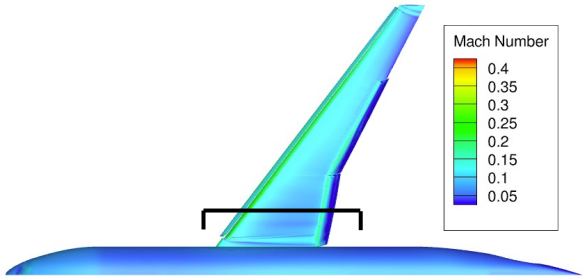
The need for efficient commercial transports requires examining and implementing technologies that can improve vehicle efficiency **throughout the flight envelope.**

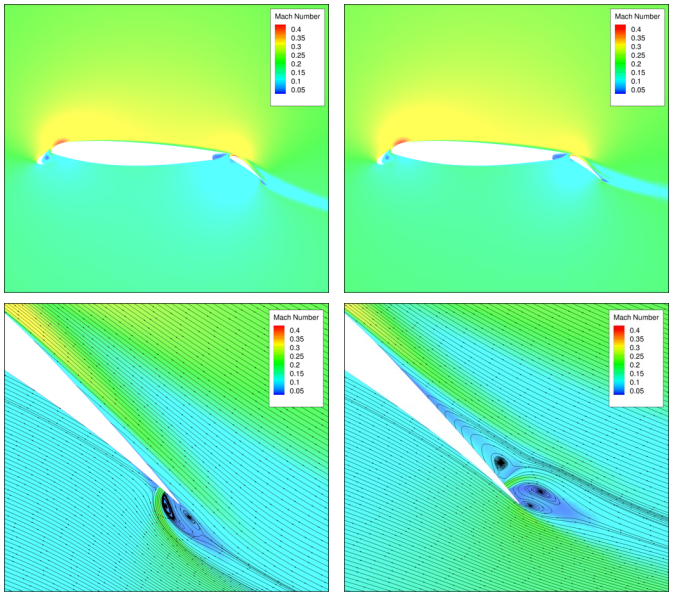
Objective

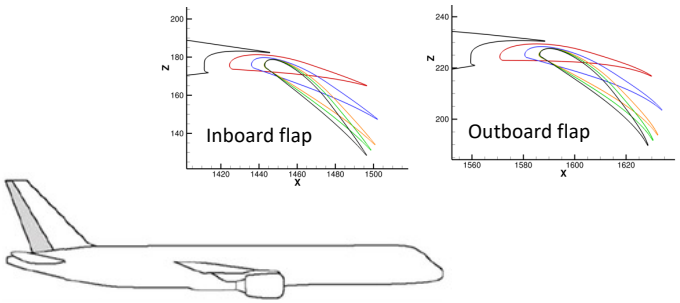
Assess potential of surface-normal pneumatic AFC, microjets, for lift control (reduction and enhancement) in the linear regime of the lift curve.

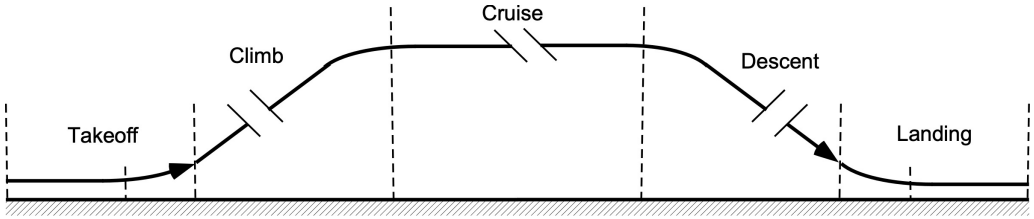
Approach

Assessment of lift control and associated wing efficiency at a range of flow conditions using both pressure-and-suction-side blowing.





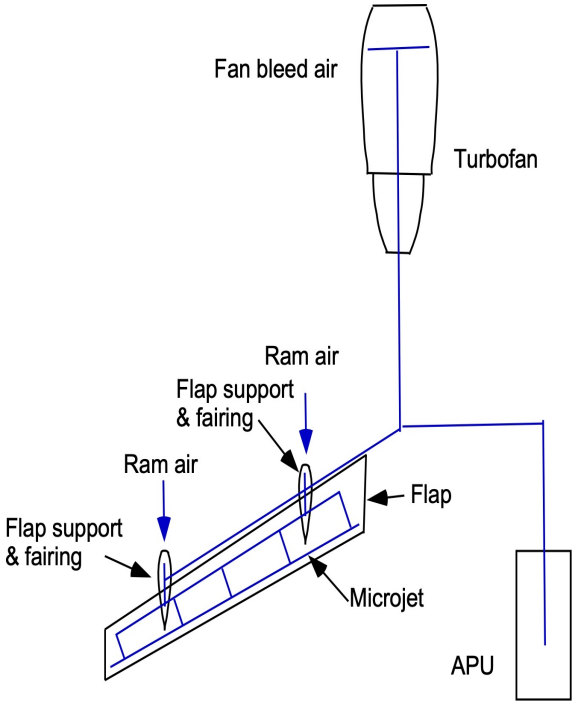




$$\alpha = 8°, \frac{Uj}{U\infty} = 1.0, C_\mu = 0.003, Y = 277.5\ [in]$$

Microjet Air Supply System Design and Analysis

- Preliminary study was conducted on the air supply system of a microjet-based AFC system in the flaps of the CRM-HL with **three sources of air** considered:
  - Bleed air from the airplane's auxiliary power unit (APU)
  - Fan bleed air from the engines
  - Ram air with intakes integrated in the flap track fairings or flap leading edges.
- Models based on the 1D compressible flow equations were derived and applied to design and analyze the air supply system
  - Focus on relatively simple systems not requiring air storage tanks or additional air compressors.

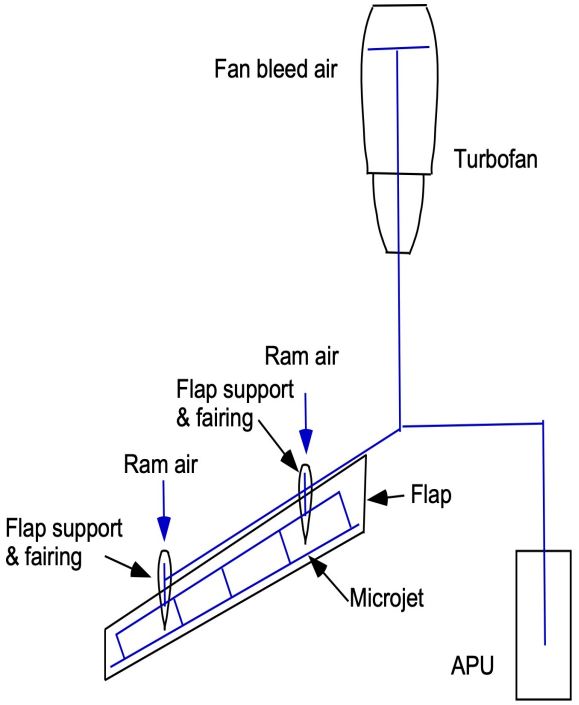


Result

- Engine fan bleed and ram air configuration
  - Provides required mass flows at required pressures for microjet-based AFC system
  - Ram air taken in at the flap LE reduces the mass flow, reduces the mass flow and therefore duct size
- APU bleed air and ram air configuration
  - Combining the ram air with APU provides the required mass flow rate
  - However there is a significant pressure difference → mixing the two can be achieved using ejector pumps
  - Model based on 1D compressible flow equations was developed to design and analyze ejectors capable of providing required mass flow rates and pressures

Microjet Air Supply System Design and Analysis

- Preliminary study was conducted on the air supply system of a microjet-based AFC system in the flaps of the CRM-HL with **three sources of air** considered:
  - Bleed air from the airplane's auxiliary power unit (APU)
  - Fan bleed air from the engines
  - Ram air with intakes integrated in the flap track fairings or flap leading edges.
- Models based on the 1D compressible flow equations were derived and applied to design and analyze the air supply system
  - Focus on relatively simple systems not requiring air storage tanks or additional air compressors.



Result

- Engine fan bleed and ram air configuration
  - Provides required mass flows at required pressures for microjet-based AFC system
  - Ram air taken in at the flap LE reduces the mass flow, reduces the mass flow and therefore duct size
- APU bleed air and ram air configuration
  - Combing the ram air with APU provides the required mass flow rate
  - However ctor pumps
  - Model ba s capable of providing

Results of preliminary study are encouraging in that effective, relatively simple AFC air supply configurations appear feasible.

Publications

- **AIAA paper 2023- 0433 (Aviation 2023)**
  - **Section: APA-42 June 15th 2023 from 1:00pm-3:00pm**
- Journal of Aircraft paper DOI: 10.2514/1.C036864
- Journal of Aircraft paper DOI:10.2514/1.C035986
- Journal of Aircraft paper DOI: 10.2514/1.C035248
- AIAA paper 2023-0433 (SciTech 2023)
- AIAA paper 2022-2535 (SciTech 2022)
- AIAA paper 2021-1192 (SciTech 2021)
- AIAA paper 2019-3498 (Aviation 2019)
- AIAA paper 2019-0590 (SciTech 2019)
- AIAA paper 2018-0559 (SciTech 2018)

Summary and Future Work

- Microjets have been proposed and demonstrated as an effective circulation control technology to enhance aerodynamic performance of high-lift systems
  - Main focus is on lift in linear regime for Vmu requirements

- Building block approach applied to research, develop and demonstrate this active flow control technology
  - 2D CFD validation/computational sensitivities for multi-element airfoils
  - 2D CFD microjet configuration studies
  - Infinite wing CFD (unswept & swept) to study impact of spanwise discontinuities on microjet effectiveness
  - Wind tunnel test of multi-element airfoil configuration studied in 2D
    - Second WT entry in April 2023
  - 3D CFD high-lift CRM
    - Validation of 2D lift enhancement trends
    - Microjet vs. flap deflection
  - Microjet system analysis
    - System feasibility and weight
    - Aerodynamic trade study

Completed
In-progress
Initiated

- Microjet technology has consistently been shown effective in the linear regime of the lift curve
  - Lift enhancement (modulation of lift performance in linear regime)
  - Lift enhancement in terms of $\Delta C_L \propto K\sqrt{C_\mu}$
  - Separation mitigation in the presence of moderate trailing edge flow separation
  - Oswald efficiency enhancement

Acknowledgment

The research reported in this presentation is funded by NASA's Advanced Air Transport Technology (AATT) project and was initially funded by Boeing Commercial Airplanes (BCA), The Boeing Company. The computing resources were provided by the NASA Advanced Supercomputing Center at NASA Ames Research Center.

The authors acknowledge the help and inputs by William Chan (NASA ARC), Thomas Pulliam (retired NASA ARC), Latunia Melton (NASA LaRC), late John Lin (NASA LaRC), Gregory Jones (NASA LaRC), Paul Vijgen (BCA), Adam Clark (BCA), Douglas Lacy (BCA) and Edward White and his research group (TAMU).